universität wien

MASTERARBEIT

Titel der Masterarbeit

„Different phenotypes of $Ca_V1.4$ loss-of-function mutations“

verfasst von

Birgit Pöhn, BSc

angestrebter akademischer Grad

Master of Science (MSc)

Wien, 2014

Studienkennzahl lt. Studienblatt:	A 066 834
Studienrichtung lt. Studienblatt:	Masterstudium Molekulare Biologie
Betreut von:	Univ. Prof. Mag. Dr. Alexandra Koschak

ACKNOWLEDGEMENTS

I am grateful to everyone who was involved in the work for this thesis. I am thankful to the members of the institute of neurophysiology and neuropharmacology for the stimulating and cooperative working atmosphere that made me enjoy working with you all.

I would especially like to thank Univ. Prof. Alexandra Koschak for supervising my thesis and giving me the opportunity to work on this interesting project. Her encouragement, guidance and scientific expertise made it a pleasure to work under her supervision.

Special thanks go to Verena Burtscher for introducing me into the world of electrophysiology and being a constant source of helpful suggestions. I want to thank Dagmar Knoflach for her valuable help and kind support in molecular biology techniques. I am thankful to Christof Kugler for helping me to get started with western blots and to Niccolò Bacchi for his assistance in site-directed mutagenesis. In addition, I would like to thank Klaus Schicker for helping out whenever unforeseen electrophysiological complications arose.

I am grateful to Markus Böhm for making my life more precious and enjoyable, giving me reason to carry on and being by my side throughout the last years.

Finally, I would like to express my deepest gratitude to my family. Without your continuing support and encouragement I would not have made it that far.

TABLE OF CONTENTS

1. INTRODUCTION

1.1. VOLTAGE-GATED CALCIUM CHANNELS (VGCCS)

Voltage-gated calcium channels mediate calcium influx upon membrane potential changes and thereby regulate processes such as contraction, secretion, neurotransmission and gene expression. They belong to a gene superfamily that also includes voltage-gated potassium and sodium channels and consist of four to five subunits (Catterall *et al.*, 2005).

The α_1 subunit is the largest subunit and harbours the pore, voltage sensor, gating apparatus and several sites involved in channel regulation (e.g. interaction sites with accessory subunits) and pharmacological modulation (like binding sites for drugs and toxins). This subunit is built up of four homologous domains (I-IV), of which each has six transmembrane segments (S1-S6). Some sites of α1 are known to serve specific functions. For example, the transmembrane segment S4 acts as voltage sensor and the pore loop between S5 and S6 determines ion conductance and selectivity. The diversity of voltage gated calcium channels is mainly due to the different types of α_1 subunits exhibiting distinct properties (Catterall *et al.*, 2005).

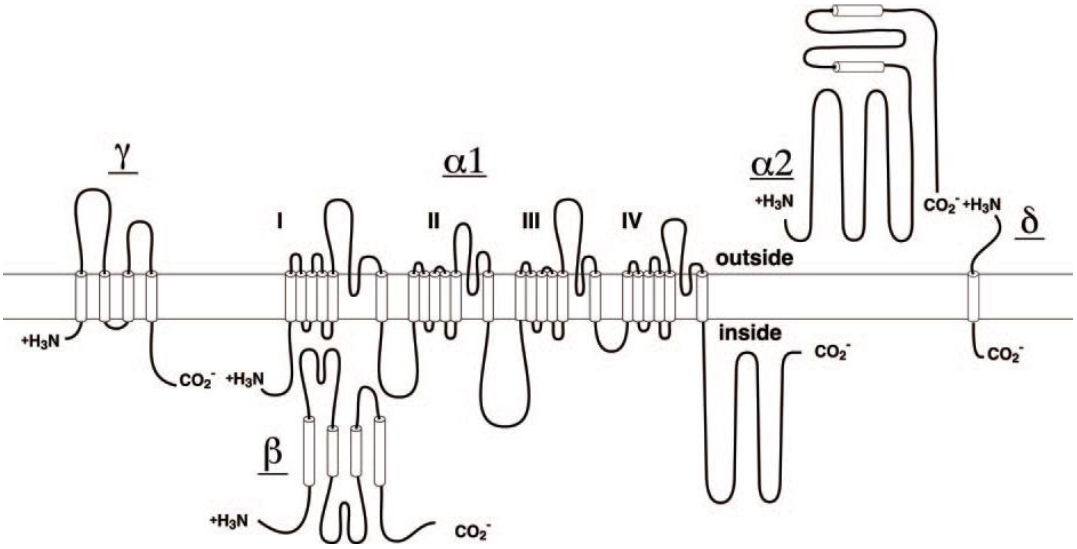

Figure 1. Subunit structure of Ca_v1 channels (Catterall *et al.*, 2005)

The α_1 subunit forms a complex with accessory subunits. The β subunit is located intracellular and enhances trafficking of the α_1 subunit to the plasma membrane, influences biophysical properties and pharmacology of the calcium channel (Dolphin, 2003; Buraei & Yang, 2010). The $\alpha_2\delta$ subunit consists of two peptide chains: δ spans through the cell membrane and α_2, which is located extracellular, is linked to δ via a disulphide-bond. It is involved in trafficking and its coexpression increases current density and influences biophysical properties of the associated channel. Additionally, $\alpha_2\delta$ serves as a drug target for the anti-epileptic and anti-nociceptive drugs gabapentin and pregabalin (Davies *et al.*, 2007; Dolphin, 2009). More recently, this subunit has been found to be involved in synaptogenesis

(Bauer *et al.*, 2010). The γ subunit is found only in skeletal muscle calcium channels ($Ca_v1.1$) (Catterall *et al.*, 2005). The assembly of subunits is shown in Fig. 1.

1.2. L-TYPE CALCIUM CHANNELS (LTCCS) (CA_V1 FAMILY)

LTCC activation is triggered by membrane depolarization. Calcium influx mediated by LTCCs is long-lasting and is blocked by organic LTCC antagonists such as dihydropyridines, phenylalkylamines and benzothiazepines (Catterall *et al.*, 2005).

$Ca_v1.1$ is expressed in skeletal muscle and is involved in excitation-contraction coupling (Catterall *et al.*, 2005). In contrast, $Ca_v1.2$ is found in cardiac and smooth muscle myocytes, endocrine cells and neurons where they play a role in excitation-contraction coupling, hormone release, regulation of transcription and synaptic integration, respectively (Catterall *et al.*, 2005). In the clinics, these channels are targets for lowering blood pressure and inducing cardiodepression. $Ca_v1.2$ was also found to mediate LTP, spatial learning and memory in the hippocampus (Striessnig *et al.*, 2010). The $Ca_v1.3$ channel is expressed in various cells like endocrine cells, neurons, cardiac atrial myocytes and pacemaker cells and cochlear hair cells. It is characterised by low-voltage activation (-65 to -40mV physiologically) and differential inactivation properties (rapidly in sinoatrial node, slow in inner hair cells) (Koschak, 2010). These properties enable it to control calcium-dependent glutamate release at cochlear inner hair cell ribbon synapses, to contribute to diastolic depolarisation in pacemaker cells at the sinoatrial node and to shape neuronal firing (Baig *et al.*, 2011). In addition, it is known to mediate LTP in the amygdala and it is involved in the consolidation of fear memory (Striessnig *et al.*, 2010).

1.2.1. $CA_V1.4$

$Ca_v1.4$ channels are almost exclusively expressed in the outer plexiform layer of the retina in rod and bipolar cells (Morgans, 2001; Morgans *et al.*, 2005). Additionally, $Ca_v1.4$ was reported to be expressed in the spinal cord, adrenal gland and in mast cells (Catterall *et al.*, 2005).

In the retina, $Ca_v1.4$ controls neurotransmitter release at ribbon synapses of retinal photoreceptors. At these synapses, glutamate is secreted in response to graded changes in membrane potential. In the dark, photoreceptors depolarize (-38 to -40mV) which enhances tonic neurotransmitter release. In contrast, light causes cGMP-gated cation channels to close, which leads to a hyperpolarization below -55mV. Therefore, Ca^{2+} -channels must activate rapidly (below -40mV) and inactivate slowly in order to couple light stimuli to tonic glutamate release from photoreceptor terminals. Recombinant $Ca_v1.4$ currents were found to meet these requirements as they activate rapidly and inactivate very slowly due to a very slow voltage dependent inactivation (VDI) and no calcium dependent inactivation (CDI) (Koschak *et al.*, 2003). $Ca_v1.4$ is thought to be the major Ca_v1 channel at ribbon synapses that induce glutamate release.

$Ca_v1.4$ is localized at the active sites of ribbon synapses of both rod and cones (Morgans, 2001; Morgans *et al.*, 2005; Liu *et al.*, 2013). A schematic view of the retina is shown in Fig. 2.

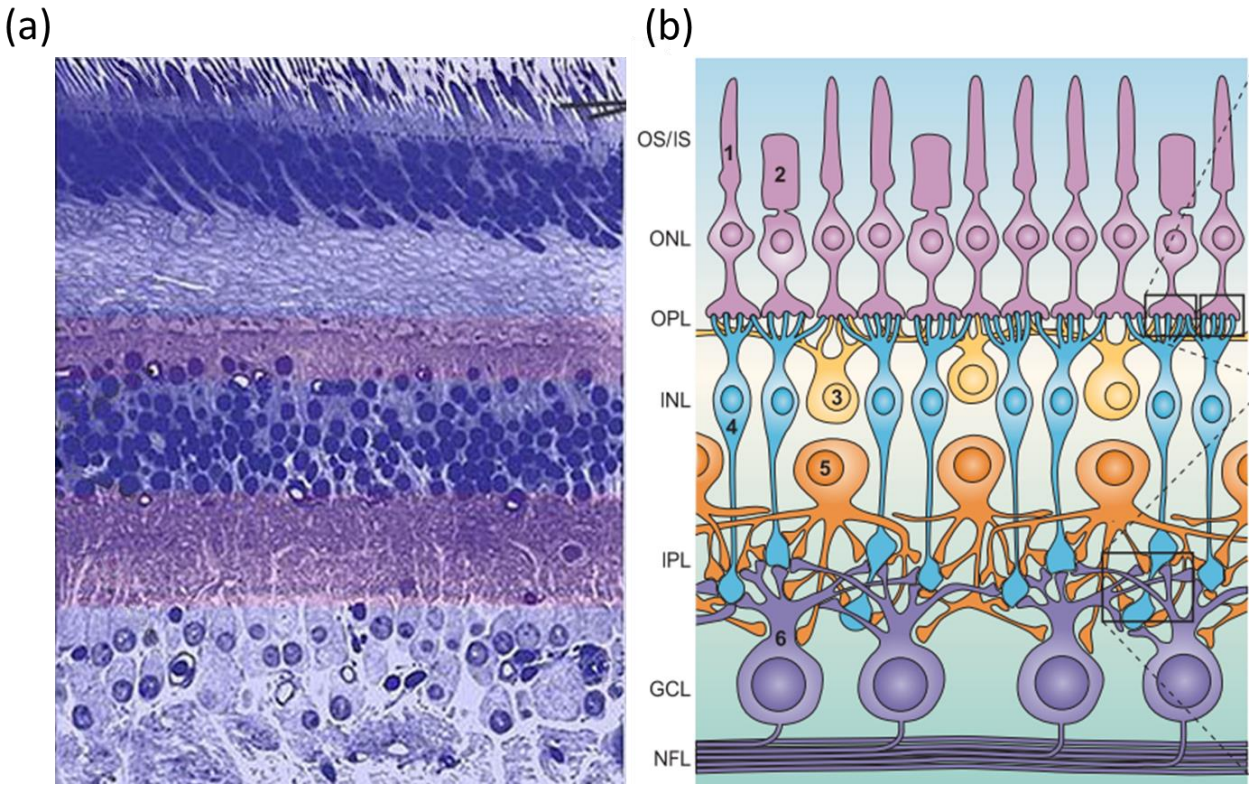

Figure 2. Organisation of the retina. (a) Light micrograph of a vertical section through central human retina. Picture adapted from http://webvision.med.utah.edu/wp-content/uploads/2011/01/husect.jpeg (b) Schematic of the mammalian retina. The different 6 types of neurons are labelled: rods (1), cones (2), horizontal cells (3), bipolar cells (4), amacrine cells (5), retinal ganglion cells (6). They are organized in layers: OS/IS, outer and inner segments of rods and cones; ONL, outer nuclear layer; OPL, outer plexiform layer; INL, inner nuclear layer; IPL, inner plexiform layer; GCL, ganglion cell layer; NFL, optic nerve fiber layer. Ribbon synapses are located in the OPL. Figure adapted from (Wässle, 2004).

Mice expressing either no (knock-out) or a truncated $Ca_v1.4$ exhibit diminished photoreceptor calcium signals and a loss of photoreceptor synapses, indicating that $Ca_v1.4$ is required for functional assembly and/or maintenance of photoreceptor ribbon synapses. In particular, the ribbons start developing, but remain immature due to abnormalities that occur after eye opening (Mansergh *et al.*, 2005; Liu *et al.*, 2013; Zabouri & Haverkamp, 2013). Proper functioning of $Ca_v1.4$ is critical for development of both rod and cone photoreceptor synapses (Zabouri & Haverkamp, 2013). Interestingly, similar developmental impairments have been observed for the I745T (IT) gain-of-function mutation. As a gain as well as a loss of function seems to affect maturation of ribbon synapses, maturation is likely to be dependent on proper activation properties of $Ca_v1.4$ (Liu *et al.*, 2013).

1.2.1.1. Gating modulation of $Ca_v1.4$

Calcium ions play a crucial role in intracellular signalling, as their cellular influx does not only depolarize the cell membrane, but calcium acts as a second messenger that affects protein phosphorylation, neurotransmitter release and gene expression (Bading, 2013). Thus, the activation of calcium channels has to be tightly regulated. This regulation is achieved via different mechanisms that adjust calcium channel properties to current needs. For example, calcium channels inactivate via 2 different mechanisms: Voltage-dependent inactivation (VDI) is solely dependent on the membrane

potential. In contrast, calcium-dependent inactivation (CDI) is caused by increasing calcium concentrations and prevents excess calcium influx. Experimentally, the calcium-dependent nature of inactivation becomes apparent when comparing calcium currents with currents recorded with barium as charge carrier. When CDI is present, calcium current decays faster than barium current. This process is dependent on calmodulin (CaM) binding to the so-called IQ and pre-IQ domains at the C-terminus of the α_1 subunit (Christel & Lee, 2012). When calcium-bound CaM is bound, it induces a conformational change that causes the so-called EF domain of the channel to induce inactivation (Wahl-Schott *et al.*, 2006).

In retinal photoreceptors, graded membrane depolarization has to be translated into sustained calcium influx, which leads to tonic glutamate release. Therefore, calcium channels mediating this release have to inactivate slowly. The $Ca_v1.4$ channel is perfectly suited for that purpose as CDI is absent and VDI is slow (Koschak *et al.*, 2003; Doering *et al.*, 2005). CDI, which is a typical feature of other LTCCs, is actively suppressed in $Ca_v1.4$ by a C-terminal modulator (CTM) (Singh *et al.*, 2006; Wahl-Schott *et al.*, 2006). In particular, the last 122 residues of $Ca_v1.4$ are required to prevent CDI and 24 amino acids of them were postulated to be critical for the suppression of CDI (Singh *et al.*, 2006). The CTM does not inhibit CDI by competing with CaM, as the CTM and CaM bind to different portions of the C-terminus. In contrast, the EF domain is an important target for the CTM and 5 residues of the IQ domain are critical for CaM binding (Griessmeier *et al.*, 2009) however this controversial (Singh *et al.*, 2006). Absence of the CTM results in CDI and a hyperpolarized shift in activation properties of about -10mV. This has been shown in truncated channels, which were artificially generated (Wahl-Schott *et al.*, 2006), identified in patients of CSNB2 (Singh *et al.*, 2006) or found to be naturally occurring splice variants (Tan *et al.*, 2012).

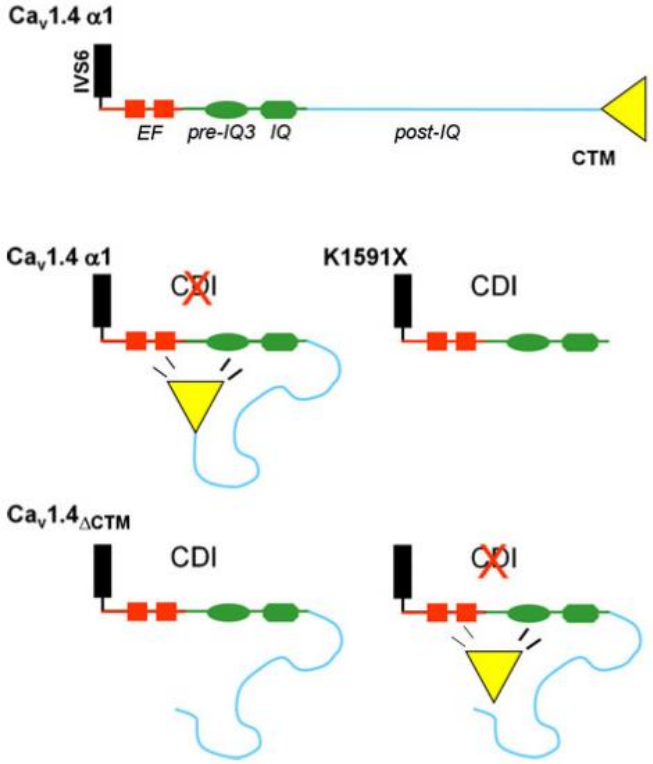

Figure 3. C-terminal modulation in $Ca_v1.4$ (adapted from (Striessnig *et al.*, 2010)). Motifs important for the regulation of CDI are depicted (red: EF hand; green: pre-IQ regions, IQ domain; yellow: CTM). The CTM suppresses CDI by interaction with upstream regions. Deletion of CTM (K1591X, Cav1.4ΔCTM) unmasks CDI, which can be rescued by coexpression of the CTM.

In addition, $Ca_v1.4$ activity is regulated by calcium binding protein 4 (CaBP4), which is a neuronal calcium sensor with structural homology to CaM. It interacts with the IQ domain and interferes with CaM binding, indicating that they may share the same binding site. Regarding CDI, CTM and CaBP4 have equivalent effects, whereas they have an opposing impact on voltage-dependent gating. Additionally, CaBP4 increases channel availability (Shaltiel *et al.*, 2012). 13.6% of $Ca_v1.4$ transcripts in the human retina are suggested to exhibit CDI, as they lack the CTM domain due to alternative splicing (Tan *et al.*, 2012). In these channels, CaBP4 may restore CTM function partially. Although this sounds plausible, it is unknown whether such mechanism is also present physiologically because neurotransmission in patients carrying e.g. the $Ca_v1.4$ truncation mutation R1827X (RX) (which still carries the potential CaBP4 binding sites (Shaltiel *et al.*, 2012)) is affected (Burtscher *et al.*, 2014).

As other L-type calcium channels, the $Ca_v1.4$ channel is sensitive to dihydropyridines such as isradipine (blocks the channel) and BayK8644 (activates the channel and shifts activation by -10mV) (Koschak *et al.*, 2003; Baumann *et al.*, 2004; McRory *et al.*, 2004). Table x lists several publications of $Ca_v1.4$ wild type activation properties. The reported V_{50} values range from -17.8 mV to 11 mV depending on the species, the expression system, the charge carrier and the protocol used. Furthermore, some working groups coexpressed the β_{2a} instead of the β_3 subunit.

Table 1. Activation properties of $Ca_v1.4$ WT. V_{50} comprises the half maximal voltage of activation. The k_{act} represents the steepness of the activation curve. SU, accessory subunit. In all experiments listed here, the α2δ-1 SU was coexpressed.

Reference	β-SU	Expression system	Charge carrier	V_{50} (mV)	k_{act} (mV)	Species	n	Comments
Burtscher and Schicker, unpublished	β_3	tsA-201	15 mM Ca^{++}	1,2 ± 0,4	9,9 ± 0,4	human	52	
McRory et al. 2004	β_{2a}	tsA-201	20 mM Ba^{++}	2,45 ± 0,54	6,67 ± 0,14	human	75	
Shaltiel et al. 2012	β_{2a}	Stable HEK line	10 mM Ca^{++}	-9,4 ± 1,9	7,9 ± 0,2	mouse	7	
			10 mM Ba^{++}	-13,4 ± 0,6	7 ± 0,2		18	
			2 mM Ca^{++}	-15,1 ± 1,36	6,9 ± 0,1		9	
Koschak et al. 2003	β_3	tsA-201	15 mM Ca^{++}	0,6 ± 2,2	-9,4 ± 0,5	human (SU rat)	6	
	β_3		15 mM Ba^{++}	-8,9 ± 0,8	-8 ± 0,4		36	
	β_{2a}			-10,7 ± 1,4	-9,5 ± 0,3		6	
Singh et al. 2006	β_3	tsA-201	15 mM Ba^{++}	-11,6 ± 0,6	ND	human	9	
			15 mM Ca^{++}	-3,5 ± 0,8	ND		7	
Hoda et al. 2006	β_3	*X. laevis* oocytes	10 mM Ca^{++}	-3,8 ± 1,3	-7,2 ± 0,3	human	5	
			10 mM Ba^{++}	-12,8 ± 0,5	-4,7 ± 0,1		20	Same data
Hoda et al. 2005	β_3	*X. laevis* oocytes	10 mM Ba^{++}	-12,8 ± 0,5	-4,7 ± 0,1	human	20	

Reference	β-SU	Expression system	Charge carrier	V_{50} (mV)	k_{act} (mV)	Species	n	Comments	
Peloquin et al. 2007	β_{2a}	tsA-201	20 mM Ba^{++}	5,2 ± 1	6,1 ± 0,4	human (SU rat)	24	Step protocol	
				11 ± 1,5	7,3 ± 0,6		6	Ramp protocol	
			2 mM Ca^{++}	0,6 ± 2	7 ± 0,5		6		
Hemara-Wahanui et al. 2005	β_{2a}	tsA-201	5 mM Ca^{++}	-10,2 ± 0,8	ND	human	9		
	β_3		20 mM Ba^{++}	-7,5 ± 0,7	ND		17		
			5 mM Ca^{++}	-14,6 ± 0,4	ND		10		
Tan et al. 2012	β_{2a}	HEK-293	5 mM Ba^{++}	-17,6 ± 0,3	-5,2 ± 0,1	human	12		
Baumann et al. 2004	β_{2a}	HEK-293	30 mM Ba^{++}	1,12 ± 1	7,92 ± 0,22	mouse	28		
			10 mM Ba^{++}	-12 ± 0,8	6,32 ± 0,1		16		
			10 mM Ca^{++}	-1,1 ± 1,8	8,1 ± 0,4		9		
	β_3		30 mM Ba^{++}	0,74 ± 2,5	10,4 ± 1,0		10		
Peloquin et al. 2008	β_{2a}	tsA-201	20 mM Ba^{++}	4 ± 2	6,4 ± 0,2	human (SU rat)	16	23°C	ramp protocol
				-8 ± 4	5,3 ± 0,3		5	37°C	
				5 ± 1	5,9 ± 0,4		15	23°C	step protocol
				-13 ± 3	3,9 ± 0,6		5	37°C	
			2 mM Ca^{++}	0 ± 1	6,1 ± 0,1		18	23°C	ramp protocol
				-9 ± 2	5,6 ± 0,3		14	37°C	

1.2.2. CHANNELOPATHIES OF LTCCS

Mutations in LTCCs lead to so-called LTCC channelopathies (Striessnig *et al.*, 2010). For example, hypokalemic periodic paralysis and malignant hyperthermia susceptibility are caused by mutations in $Ca_v1.1$. Mutations in the α_1 subunit of $Ca_v1.2$ are associated with a severe disorder called Timothy syndrome that is very likely to cause childhood death (Splawski *et al.*, 2005). A loss-of-function mutation in $Ca_v1.3$ leads to bradycardia and congenital deafness (Baig *et al.*, 2011). In addition, some somatic mutations in $Ca_v1.3$ occurring in aldosterone-producing adenomas cause hypertension by increasing aldosterone secretion (Azizan *et al.*, 2013). Various mutations in $Ca_v1.4$ give rise to incomplete congenital stationary night blindness (CSNB2), which will be discussed in detail below (Stockner & Koschak, 2013).

1.2.2.1. Incomplete congenital stationary night blindness type 2 (CSNB2)

CSNB2 is an X-linked disorder that can be caused by several different mutations in the *CACNA1F* gene coding for the $Ca_v1.4$ α subunit. It is characterised by variable and mostly mild clinical symptoms like low visual acuity, myopia, nystagmus and night blindness. However, some of these symptoms may be absent. The eye fundus is normal, but the electroretinogramm (ERG) reveals dim scotopic, negative bright-flash ERG with large a-waves and severely reduced b-waves. Additionally, oscillatory potentials are missing (Schubert & Bornschein, 1952; Miyake *et al.*, 1986). These observations correspond with a defect in neurotransmission between photoreceptors and second-order neurons.

To date, about 100 different mutations of the *CACNA1F* gene (coding for the α1 subunit of $Ca_v1.4$) have been identified in CSNB2 patients (Bech-Hansen *et al.*, 1998; Strom *et al.*, 1998; Boycott *et al.*, 2001; Nakamura *et al.*, 2001; Wutz *et al.*, 2002; Jacobi *et al.*, 2003; Hemara-Wahanui *et al.*, 2005; Zeitz *et al.*, 2005, 2009). These include truncations, missense mutations, deletions or insertions and mutations that affect splicing. Several of these mutants have been characterised in electrophysiological experiments. Many of them lead to changes in gating properties. All mutations mentioned here are numbered according to GenBank accession number AJ224874.

For example, the W1440X truncation was found to be not expressed on the protein level in transfected tsA-201 cells (Hoda *et al.*, 2005). However, McRory et al. 2004 reported that there was expression and no significant difference concerning activation, inactivation or conductance properties compared to wild type. These controversial results may also be due to the fact that different clones of $Ca_v1.4$ were used in these studies. Hoda et al. 2006 reported that the mutations R508Q and L1364H display a reduced expression in tsA-201 cells. In contrast, some mutated channels are expressed at the same level as wild type channels, but are non-functional. For example, no current could be detected for the G1007R, R1049W (Peloquin *et al.*, 2007) and the S229P (Hoda *et al.*, 2005) missense mutation. It is possible, that these mutations disturb protein trafficking and that the channel is not targeted to the plasma membrane. L1068P only yielded current in the presence of the L-type calcium channel activator BayK8644 (Hoda *et al.*, 2005). CSNB2 can also be caused by mutations which lead to a gain-of-function of $Ca_v1.4$, as seen for G369D (Hoda *et al.*, 2005). It changes inactivation gating and shifts V_{50} to more negative voltages, leading to an overall gain-of-function. Similar effects were discovered in the I745T substitution. It is located in domain II segment 6 and leads to a negative shift

in the voltage dependence of activation. Additionally, this mutant exhibits slower inactivation kinetics (Hemara-Wahanui *et al.*, 2005). However, for some mutations (G663D and A917D, investigated by McRory et al. 2004), no differences in expression or gating properties compared to wild type have been found.

More recently, studies on $Ca_v1.4$ KO and $Ca_v1.4^{I745T}$ knock-in mice have uncovered the importance of Cav1.4 functionality in the development of ribbon synapses. These results imply that CSNB2 may be the result of impaired development of photoreceptor synapses that is caused by functional changes in $Ca_v1.4$ (Knoflach *et al.*, 2013; Liu *et al.*, 2013; Zabouri & Haverkamp, 2013).

1.3. AIM OF THIS STUDY

CSNB2 results from a wide spectrum of different dysfunction phenotypes in $Ca_v1.4$ channels. It is not known how these different changes contribute to the same disease.

In this study, I investigated 3 prototypical mutations of $Ca_v1.4$, exhibiting a loss-of-function (L216R), a gain of function (I745T) and a C-terminal truncation (R1827X) phenotype (Fig. 4). I have characterised these mutations via whole-cell patch clamp in order to elucidate how they affect the channel's biophysical properties.

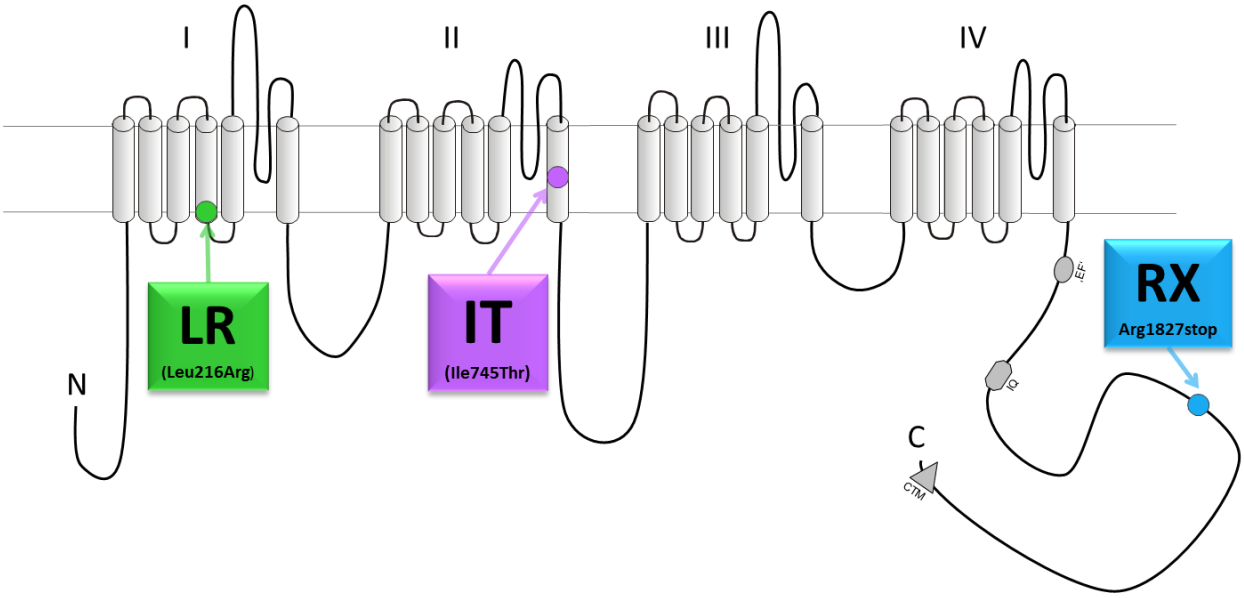

Figure 4: Topology of the $Ca_v1.4$ channel. Locations of mutations that were investigated are indicated.

2. MATERIAL AND METHODS

2.1. MOLECULAR BIOLOGY AND CELL CULTURE

2.1.1. TRANSFORMATION AND PLASMID PREPARATION

E. coli were cultivated in LB medium (10g/l peptone, 5g/l yeast extract, 10g/l NaCl) or LB agar (15g agar/l LB medium), pH 7.3. 100ng of the desired plasmid were added to competent E. coli cells and the bacteria were heat-shocked at 42°C for 90s. After adding 1ml of LB medium, the vials were incubated on a shaker at 37°C for 1h at 300rpm. 50µl of the culture was plated on agar plates containing the appropriate antibiotic to select for transformed cells and they were allowed to grow over night at 37°C. The next day in the morning, single colonies were picked, transferred to tubes containing 5ml LB medium with antibiotic and incubated on a shaker at 37°C at 200rpm. In the evening, 1ml (2ml for low-copy plasmids) of the culture was used to set up the main culture. It was allowed to grow until the next day at 37°C and 200rpm. NucleoBond® Xtra kit (Macherey-Nagel) was used for plasmid isolation according to the manufacturer's instructions. DNA was isolated via a NucleoBond Finalizer and eluted in 400µl TRIS buffer. DNA concentration was determined with a nanophotometer (Implen). For quality control, plasmids were digested with appropriate restriction enzymes and the lengths of the resulting fragments were checked by agarose gel electrophoresis.

2.1.2. CELL CULTURE AND TRANSFECTION

2.1.2.1. Splitting of tsA-201 cells

tsA-201 cells were cultivated at 37°C and 10% CO_2 in DMEM high glucose (4500mg/l) medium supplemented with 10% heat-inactivated FCS and 2mM L-Glutamine. When reaching approximately 80% confluence, cells were washed with PBS and incubated with 0.25% trypsin solution pre-warmed to 37°C until the cells detached, which was facilitated by tapping against the flask. After the cells had detached, trypsin activity was stopped by adding the double volume of culture medium. The resulting cell suspension was centrifuged for 4min at 80G at room temperature. The supernatant was removed and the cell pellet was resuspended in 1ml of culture medium. Aliquots of this cell suspension were transferred into prepared flasks or dishes containing culture medium. Passage number did not exceed 30 passages.

2.1.2.2. Transfection of tsA-201 cells

Cells were transfected by either TurboFect reagent (Thermo Scientific) according to the manufacturer's instructions or standard calcium-phosphate transfection method. GenBank accession number of $Ca_v1.4$ α_1 was JF701915. The day before transfection, cells were plated into the appropriate dishes. For the transfection with IT α_1, medium was changed to calcium-free medium prior to transfection. For mock-transfection, the α_1 subunit was omitted. The amount of DNA used is depicted in Tab 2.

Table 2: Amount of DNA used for transfection (all given in µg)

plasmid	TurboFect				Calcium Phosphate	
	25cm² flask	35mm dish	10 cm dish	20cm dish	25cm² flask	35mm dish
α1	0.6	0.25	1	3.5	1.5	1.125
β3	0.6	0.25	1	3.5	1	0.625
α2δ-1	0.6	0.25	1	3.5	1.25	0.875
pUC	1.2	0.5	2	7	1.25	1.125
eGFP	0.1	0.025	0.025	0.1	0.25	0.2
Serum-free medium (µl)	500	200	500	3500	--	--
TurboFect (µl)	6	3	12	40	--	--

For transfection via TurboFect reagent, the DNA was diluted in serum-free medium and TurboFect reagent was added. The mixture was incubated for 20min at room temperature and was then applied to the cells dropwise.

For calcium phosphate transfection, 250mM $CaCl_2$ solution and HEBS buffer were thawed and cooled down to room temperature. $CaCl_2$ was added to the appropriate amount of DNA to reach a final volume of 100µl (35mm dishes)/250µl (25cm^2). The DNA/$CaCl_2$ mix was added to the same volume of HEBS in a drop-wise manner and incubated for 20min at room temperature. Afterwards, the mix was applied to the cells drop by drop. The calcium phosphate precipitate was checked under the microscope and the medium was changed after 6-8h.

Table 3. Preparation of HEBS buffer and $CaCl_2$ solution

HEBS buffer	
NaCl	8g
HEPES	4.75g
KCl	0.375g
Na_2HPO_4 x $2H_2O$	0.125g
Dextrose x H_2O	1.19g
H_2O	Fill up to 500ml

Adjust the pH to 7.05 using 1M NaOH.

$CaCl_2$ [250mM]	
$CaCl_2$ x $2H_2O$	18.4g
H_2O	Fill up to 500ml

2.1.3. WESTERN BLOT

2.1.3.1. Cell treatment for turnover experiments

Previously (1-2 days ago) transfected tsA-201 cells were treated with 10µM cycloheximide (CHX) for 2 and 4 hours. In addition, cells were treated with 10µM CHX and 5µM MG-132 concomitantly for 4 hours.

2.1.3.2. Cell lysis and protein isolation

Transfected tsA-201 cells were detached with PBS and centrifuged for 5min at 1500rpm at 4°C. The supernatant was discarded and lysis buffer (1ml for 5 dishes) added. The suspension was incubated on ice for 15min. Afterwards, the pellet was resuspended via pipetting and pressing through a cannula (d=0.4mm). The resulting solution was centrifuged for 20min at 3000rpm and 4°C. The supernatant was transferred into an ultracentrifuge tube and centrifuged at 110000G and 4°C for 20min. The supernatant was discarded and the pellet was incubated on ice for 5min. Lysis buffer (100µl for 5 cell culture dishes) was added to the pellet and stored on ice for 60min. Afterwards, the pellet was resuspended with a cannula (d=0.4mm). The suspension was aliquoted, shock-frozen with liquid N_2 and stored at -80°C.

Table 4. Composition of lysis buffer

Lysis buffer	
Tris/HCl pH 7.4 [1M]	125µl
Aprotinin [1mg/ml]	12.5µl
Trypsin inhibitor [100mg/ml]	12.5µl
Pepstatin A [1mM in EtOH]	12.5µl
Benzamidin [0.1M]	62.5µl
PMSF [40mM in EtOH]	62.5µl
Iodacetamid [0.1M]	250µl
Leupeptin [1mg/ml]	12.5µl
H_2O	11.95ml

2.1.3.3. Protein quantification

Protein was quantified using the method of (Lowry *et al.*, 1951). Standards were prepared from a 2mg/ml albumin standard (Thermo Scientific) diluted in H_2O (concentrations ranging from 10-200 µg/µl in intervals of 10 µg/µl). The protein sample was diluted (1:20, 1:40 and 1:80) and 3 vials with 100 µl H_2O (blind probes) were prepared. 100 µl of the standards/sample/water were mixed with 100 µl of 0.1% SDS and 1ml of Folin I was added. After 10 min, 100 µl of freshly prepared Folin II (Folin & Ciocalteau's phenol reagent 1:1 diluted with H_2O) was added (in the dark) and stored for 30 min in a dark place. Absorption was measured at 750 nm.

Table 5. Composition of Folin I solution

Folin I	
Na_2CO_3	20g
NaOH [0.1M]	980ml
Potassium-sodium-tartrate x 4 H_2O	0.2g
H_2O	20ml
$CuSO_4$	0.1g

2.1.3.4. SDS-PAGE

The gel casting device (BioRad Mini PROTEAN) was washed thoroughly with 70% EtOH and H_2O. Both the glass plates and the comb had a thickness of 1.5mm. The device was assembled and was checked for leakage with H_2O. The resolving gel (6% PAA) was prepared according to table x, pipetted between the plates quickly and overlaid with isopropanol in order to obtain a sharp edge. After polymerisation, isopropanol was discarded. The stacking gel (4% PAA) was prepared (table x), pipetted onto the resolving gel and the comb (10 wells) was inserted.

Table 6. Resolving gel for SDS-PAGE

Resolving gel (6% PAA)	
H_2O	6ml
Tris/HCl, pH=8.8 [2M]	1.875ml
SDS (20%)	50µl
Acrylamide/Bisacrylamide (30%/0.8%)	2 ml
APS (10%)	80µl
TEMED	8µl

Table 7. Stacking gel for SDS-PAGE

Stacking gel (4% PAA)	
H_2O	3.35ml
Tris/HCl, pH=6.8 [0.625M]	1ml
SDS (20%)	25µl
Acrylamide/Bisacrylamide (30%/0.8%)	665µl
APS (10%)	40µl
TEMED	4µl

The gel was mounted into the gel running device (BioRad Mini PROTEAN Tetra system), the comb was carefully removed and the chamber was filled with 1x running buffer. In order to remove gel debris, each slot was rinsed with running buffer by pipetting up and down.

30µg protein was loaded for each probe in a total volume of 30µl. For that purpose, the volume of cell lysate containing 30µg of protein was calculated, it was filled up with H_2O to 24µl and 6µl sample loading buffer (5x) was added. The lysates were incubated at 57°C for 15min for denaturation. 12µl of a marker (Page ruler Plus prostained Protein ladder or Spectra Multicolor Broad Range Protein Ladder, Thermo Scientific) was used. Unoccupied slots were filled with 1x loading buffer. Gels were run at constant voltage for 20min at 100V and 45-50min at 140V.

Table 8. Composition of sample loading buffer

Sample loading buffer	Amount for 5x	5x	1x
Tris/HCl, pH=6.8 [2M]	3.9ml	0.3125M	62.5mM
SDS	5g	20% (w/v)	4% (w/v)
Glycerol	12.5ml	50% (v/v)	10% (v/v)
DTT (Dithiothreitol)	0.193g	50mM	10mM
Bromphenole blue	A tiny crystal	--	--
H_2O	Fill up to 25ml	--	--

Table 9. Composition of running buffer

8x Running buffer stock	Amount for 8x	8x	1x
Tris	24.28g	200mM	25mM
Glycine	114.86g	1.53M	192mM
H_2O	Fill up to 1l	--	--

1x Running buffer	
8x Running buffer stock	125ml
SDS (20%)	5ml
H_2O	Fill up to 1l

2.1.3.5. Blotting and Analysis

4 sponges, 2 filter papers (blotting paper 330g/m^2, Hartenstein Laborbedarf GmbH) and a nitrocellulose (NC) membrane (Protran BA 85, Whatman) in the size of the gel were soaked in transfer buffer. The blot sandwich was prepared in the following order: 2 sponges – 1 filter paper – gel – NC membrane – 1 filter paper – 2 sponges. Air bubbles were carefully removed and the blot sandwich was inserted into the transfer chamber. The device was filled with transfer buffer and a cooling block and run at 100V for 90min (120min for 2 gels) on ice.

Table 10. Composition of transfer buffer

Transfer buffer	
8x Running buffer stock	125ml
Methanol	200ml
H_2O	Fill up to 1l

To check for successful transfer, the gel was stained with staining solution for 2h, then incubated in H_2O overnight. The next day, destaining solution was applied for 90min and the gel was again laid into water.

Table 11. Composition of staining and destaining solution

Staining solution	
Brilliant blue	2g
Acetic acid	75ml
Ethanol (96%)	500ml

Destaining solution	
Acetic acid	100ml
Ethanol (100%)	400ml
H_2O	500ml

The NC membrane was incubated in blocking buffer at room temperature for 2h under slight agitation. The blot was then cut in two pieces at the 70kDa marker. The part with higher mass proteins was incubated with the antibody for $Ca_v1.4$ and the part with lower mass proteins was incubated with the alpha tubulin antibody. The blocking buffer was removed and replaced by the primary antibody solution (antibody diluted in blocking buffer) and incubated over night at 4°C. The next day, the membrane was washed 5 times for 5 minutes with washing buffer. Afterwards, the washing buffer was replaced by the secondary antibody solution (diluted in blocking buffer) and incubated for 2h at room temperature. Subsequently, the membrane was washed again 5 times with washing buffer for 5min. ECL solutions 1 and 2 (Pierce ECL Western Blotting Substrate, Thermo Scientific) were mixed in a 1:1 ratio and added to the membrane. After 2min of incubation, the membrane was carefully placed in a film cassette. In the dark room, a film (High performance chemiluminescence film, GE Healthcare Limited) was mounted on the membrane and exposed for different time frames. The films were then developed using a developing device (Agfa).

Table 12. Compostion of washing buffer and blocking buffer

Washing buffer		
Tris/HCl, pH=7.4 [1M]	20ml	20mM
NaCl	9g	150mM
Triton X-100	5ml	0.5%
Tween 20	1ml	0.1%
H_2O	Fill up to 1l	

Blocking buffer		
Non-fat dry milk	5g	5%
Gelatine powder	0.2g	0.2%
Washing buffer	Fill up to 100ml	--

Table 13. Antibodies used in this study

Antibodies	Company	Catalogue number	species	dilution
pan anti-$Ca_v1.x$	Millipore	AB5150-50UL	rabbit	1:1,000
Anti-rabbit IgG peroxidase conjugated	Sigma	A0545	goat	1:10,000
Anti-Beta-tubulin	AbFrontier	LF-MA20056	mouse	1:2,000
Anti-mouse IgG peroxidase conjugated	GE Healthcare	NA931V	sheep	1:10,000

Films were scanned (in greyscale) and analysed with ImageJ. For that purpose, rectangles were drawn over the respective lanes and plotted. The area under the curve (AUC) of the peak of interest was quantified.

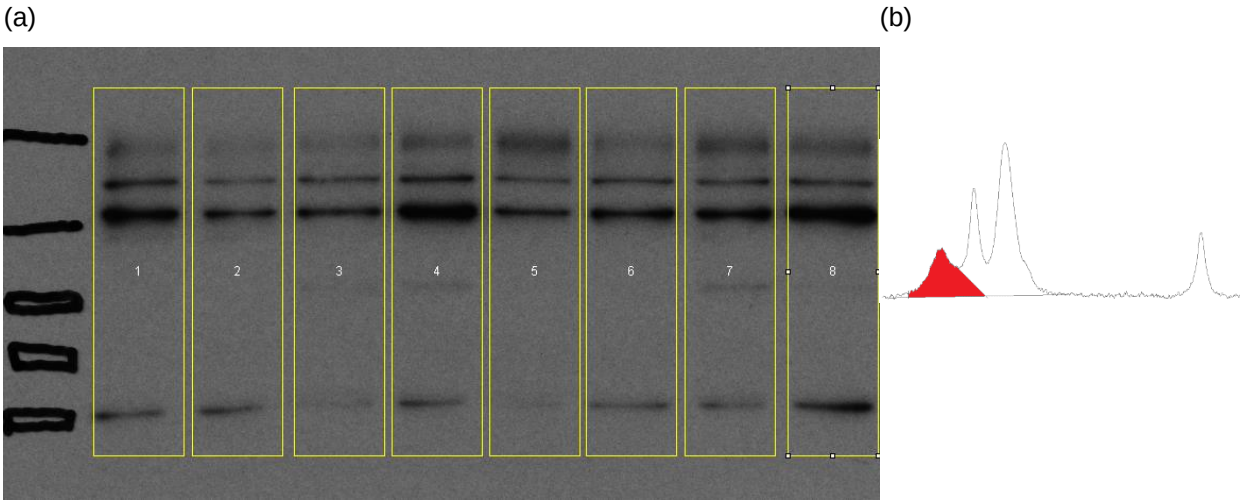

Figure 5. Procedure for quantification of western blots. (a) Screenshot of the drawn rectangles in ImageJ. (b) Representative plot of a lane. The AUC of the specific $Ca_v1.4$ band is highlighted in red.

In order to check for successful and uniform transfer, membranes were stained with Ponceau S for 5 min and excess solution was removed by shortly rinsing them with H_2O. The blots were scanned as described previously for western blot films.

2.1.4. *SITE-DIRECTED MUTAGENESIS*

The pGFP+_Ca_v14_K1911-1934 plasmid expresses a C-terminal peptide (K1911-1934) of $Ca_v1.4$ fused to eGFP. However, in our construct a frameshift occurred at the junction between eGFP and the K1911-1943 peptide that was corrected by site-directed mutagenesis. In addition, a stop codon was created at the end of the peptide. Fig. 6 shows the concept for these corrections.

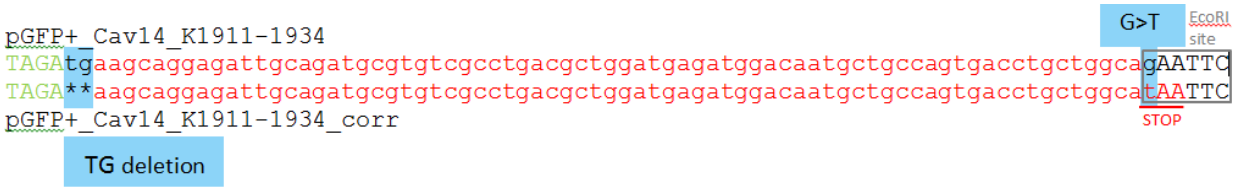

Figure 6. Concept for site-directed mutagenesis of the pGFP+_Cav14_K1911-1934 plasmid. The C-terminus of the eGPF sequence is shown in green, whereas the K1911-1934 fragment is depicted in red. The anticipated changes are highlighted in blue. The G>T exchange destroys an EcoRI site, which was used to identify mutated clones.

2.1.4.1. Design of mutagenic primers

For each mutation, a forward and a reverse primer with the desired mutation was designed. The primers should have 25 to 45 bases in length and a melting temperature of ≥ 78°C. The mutation should be located in the middle of the primer with 10-15 correct bases on each side. Furthermore, the GC content should be at least 40% and the primers should terminate in one or more C or G bases.

The melting temperatures (T_m) were calculated with the following formulas:
For mismatching primers: Tm = 81.5 + 0.41 (%GC) - 675/N - % mismatch
For insertions or deletions: Tm = 81.5 + 0.41 (%GC) 675/N (N does not include bases which are inserted/deleted)

Table 14. Mutagenic primers used for site-directed mutagenesis

Primer name	sequence	N	% GC	T_m (°C)
TG del fwd	GCAGGTCGACTCTAGAAAGCAGGAGATTGCAG	32	53.1	80.771
TG del rev	CTGCAATCTCCTGCTTTCTAGAGTCGACCTGC			
G>T fwd	CAGTGACCTGCTGGCATAATTCAATCGATGGCC	33	51.5	78.9
G>T rev	GGCCATCGATTGAATTATGCCAGCAGGTCACTG			

Primers were purchased at Microsynth AG. The lyophilized primers were dissolved in ddH_2O to obtain a concentration of 100µM, which was further diluted in a 1:10 ratio in order to obtain a 10µM working stock.

2.1.4.2. PCR

Table 15. Ingredients for PCR mix.

Reagent		G>T	TG del
ddH_2O	Fill up to 50µl	36.5µl	37.5µl
Pfu Ultra Hotstart Polymerase buffer (10x)	5µl	5µl	5µl
DNA template	10 ng	5µl	3.5µl
Fwd primer [10µM]	125 ng	1.25µl	1.25µl
Rev primer [10µM]	125 ng	1.25µl	1.25µl
dNTP [2mM]	1mmol	0.5µl	0.5µl
Pfu Ultra Hotstart DNA Polymerase	1µl	1µl	1µl

Table 16. PCR program for site-directed mutagenesis.

Step	Temperature (°C)	Duration (min)	Cycles
Initial denaturation	95	1:00	1x
Denaturation	95	0:50	18x
Annealing	60	0:50	
Elongation	68	5:30	
Final elongation	68	7:00	1x
	12	forever	

2.1.4.3. DpnI digestion

DpnI is a restriction enzyme that recognizes and cuts methylated DNA. As only the parental, i.e. non-mutated plasmids in the PCR tube are methylated, this enzyme was used to degrade the non-mutated DNA. For that purpose, 1µl of DpnI enzyme was added to the PCR product and it was incubated for 1h at 37°C.

2.1.4.4. Transformation and picking of clones

After DpnI digestion, XL-1 blue cells were transformed. For that purpose, 10µl of the PCR product was added to 50µl freshly thawed XL-1 blue cells. H_2O was used as a negative control. After 30min incubation on ice, the bacteria were heat-shocked for 90s at 42°C. 1ml of NZY^+ broth was added and the suspension was incubated at 37°C and 300rpm for 1h. The bacterial suspension was centrifuged, 500µl of the supernatant was removed and the pellet was resuspended in the residual supernatant. All of the suspension was spread onto LB agar plates with ampicillin in various dilutions (e.g. 200µl, 100µl, 50µl).

Table 17. Compositon of NZY+ broth

NZY^+ broth	
NZ amine (casein hydrolysate)	10 g
Yeast extract	5 g
NaCl	5 g
H_2O	Fill up to 1l

Adjust pH to 7.5 using NaOH, autoclave and add:

$MgCl_2$ [1M], filter-sterilized	12.5 ml
$MgSO_4$ [1M], filter-sterilized	12.5 ml
Glucose [2M], filter-sterilized	10 ml

The next day, colonies were picked and inoculated in 5ml LB medium supplemented with ampicillin and incubated at 37°C and 200rpm for 24h.

2.1.4.5. Mini prep and glycerol stocks

2ml of each culture was centrifuged at 8000rpm for 2min at room temperature. Supernatants were discarded and DNA was isolated using Thermo Scientific GeneJET Plasmid Miniprep Kit according to the manufacturer's instructions. DNA was eluted in 50µl elution buffer and concentration was determined with a nanophotometer (Implen). The remaining 3ml of culture were used to prepare glycerol stocks (800µl culture + 200µl glycerol), that were stored at -80°C.

2.1.4.6. Check for successful mutagenesis

We started with the G>T substitution, as this mutation could be easily checked by a EcoRI digest (Fig. 7). A successfully mutated clone (#10 in Fig. 7) was then picked for the TG deletion and obtained clones were sequenced by LGC genomics. The sequencing primer CCTGTCCACACAATCTGCCC was binding 140bp upstream of the mutation sites. The sequence showed 100% alignment.

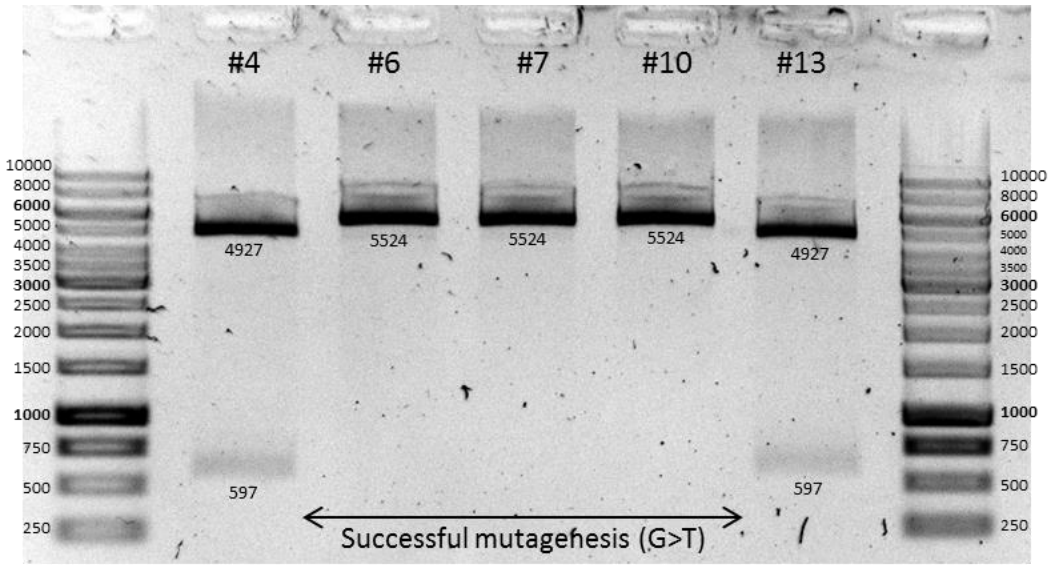

Figure 7. Restriction digest of clones after the first mutation step (G>T). 200ng DNA was digested with EcoRI and HpaI and was separated on a 0.8% agarose gel that was run at 75V for 45min. Mutagenesis was successful in clones #6, #7 and #10. #10 was selected for the second mutation (TG deletion).

2.2. ELECTROPHYSIOLOGY

The day after transfection, cells were splitted into 35mm dishes previously coated with poly-D-lysine (2ml medium per dish) and cultivated at 30°C and 5% CO_2 until they were recorded (after 12-48h). Electrodes were pulled from glass capillaries (Borosilicate glass; 1.5mm diameter, 0.32mm wall thickness; Science products) using a micropipette puller (P97, Sutter Instruments, USA) and had a resistance of 2-5MΩ. Cells were recorded in whole-cell mode using Axopatch 700B amplifier (Molecular Devices, USA). Used intracellular and extracellular solutions are depicted in table x. 15mM Ca solution was used as bath solution. The respective external solution used for recording was superfused by a pressure-driven (30-70mmHg) perfusion system. (±)-BayK 8644 (BayK, Sigma Aldrich, B112, racemic) was dissolved in 15mM Ca^{2+} solution together with dimethyl sulfoxide (final concentration 0.1%).

Table 18. Composition of intracellular and extracellular solutions used in electrophysiological recordings

Int. CsCl	**Ext. 15mM Ca^{2+}**	**Ext. 15mM Ba^{2+}**	**Ext. 16mM Mg^{2+}**
135mM CsCl	150mM Choline-Cl	150mM Choline-Cl	150mM Choline-Cl
10mM HEPES	10mM HEPES	10mM HEPES	10mM HEPES
10mM EGTA	15mM $CaCl_2$	15mM $BaCl_2$	16mM $MgCl_2$
1mM $MgCl_2$	1mM $MgCl_2$	1mM $MgCl_2$	

Cells were recorded 2-3 days after transfection in whole-cell mode. In order to obtain current-voltage (I-V) relationships, cells were clamped to -98mV and then depolarized to -78mV in 10mV steps up to 52mV, each voltage pulse lasting for 300ms (RX recordings) or 50ms (LR and IT recordings) and fitted to the equation $I = (G_{max}*(V-V_{rev}))/(1+\exp((V_{50}-V)/k_{act}))$, where G_{max} is the maximum conductance, V_{rev} is the reversal potential, V is the membrane potential, V_{50} is the half maximal activation voltage and k_{act} is the slope factor. Activation curves were calculated using the maximum conductance (G_{max}), the reversal potential (V_{rev}), the membrane potential (V) and the maximum current (I_{max}) of the respective sweep and were fitted to the Boltzmann sigmoidal equation $I_{normalized}$=Bottom+(Top-Bottom)/(1+exp((V_{50}-X)/k_{act}). Calcium dependent inactivation (CDI) was quantified as the current remaining after 250ms pulse duration (expressed as fraction of the peak current amplitude r_{250}). Gating currents were recorded using 16mM Mg^{2+} solution supplemented with 15µM $GdCl_3$ to block calcium currents. Cells were clamped to -98mV and depolarized to potentials in the range from -78 to +62mV in 10mV increments for 20ms. In contrast to sigmoidal gating currents, capacitive transients showed linear voltage dependence and were therefore excluded from analysis.

2.3. DATA ANALYSIS AND STATISTICS

Data were analysed using Clampfit 10.2, Microsoft Excel 2010 and GraphPad Prism 5. All data are presented as mean ± SEM for the indicated number of experiments (n).

Difference of gating charge transfer was evaluated using the Mann Whitney U test. P values <0.05 were considered to be statistically significant.

3. RESULTS

3.1. THE $Ca_V1.4$ WILD TYPE CHANNEL

$Ca_v1.4$ channels are slow inactivating, as VDI is slow and CDI is absent due to an intrinsinc regulatory mechanism, called C-terminal modulation (Singh *et al.*, 2006; Wahl-Schott *et al.*, 2006). Barium as charge carrier yields larger currents than calcium (Fig. 8 b, d). The calcium channel activator BayK8644 (BayK) does not only elevate current density, but also shifts the activation curve by about -10mV to more hyperpolarised potentials (Fig. 8, Tab. 19) (Koschak *et al.*, 2003).

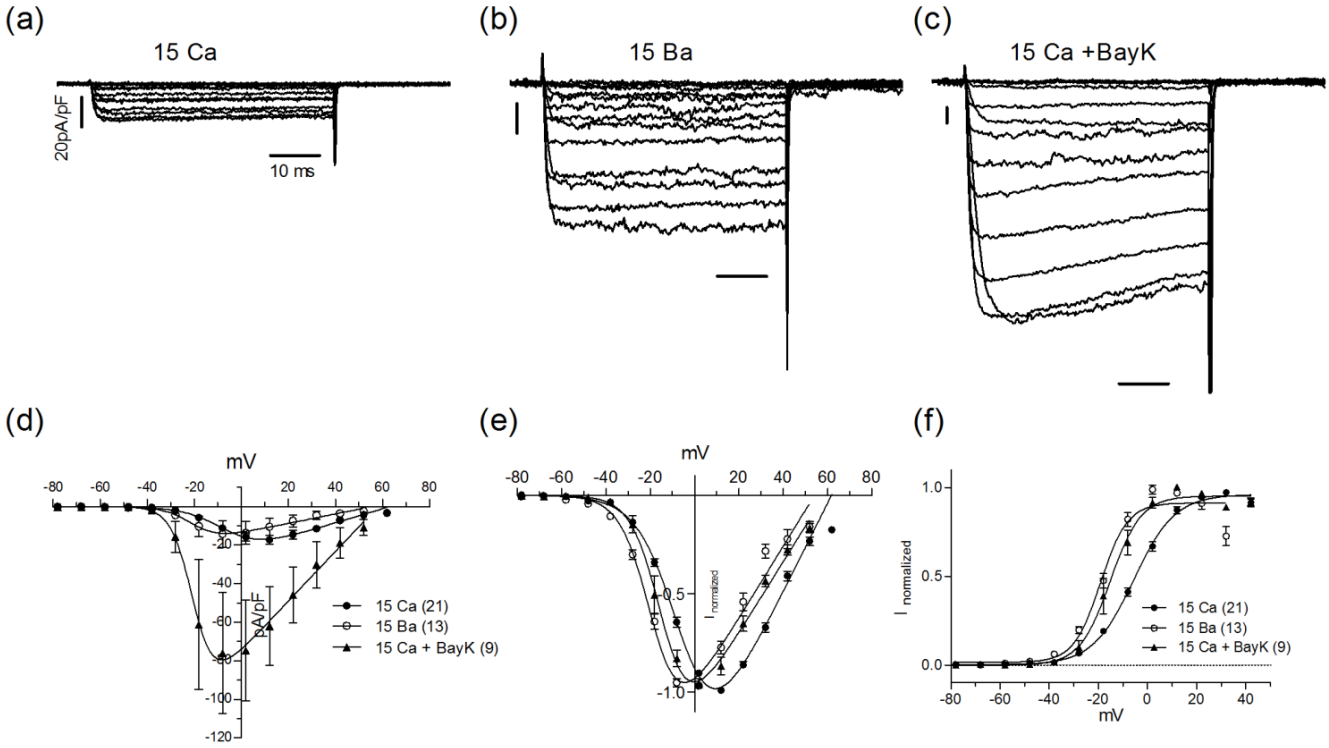

Figure 8. Representative currents and biophysical properties of the $Ca_v1.4$ WT channel. (a, b, c) representative currents recorded from tsA-201 cells transiently transfected with $Ca_v1.4$ and the accessory subunits β_3 and $\alpha_2\delta$-1 with the charge carriers indicated. (d) current densities recorded with 15 mM Ca^{2+} (filled circles), 15mM Ba^{2+} (open circles) and 15mM Ca^{2+} +3µM BayK (triangles). (e) normalized current-voltage relationship of data shown in (d). Colour code is the same as in (d). (f) Voltage-dependent activation properties of the $Ca_v1.4$ WT channel. Data are presented as means ± SEM and the number of experiments is given in parentheses.

Table 19. Biophysical parameters of wild type channels using different charge carriers. Data are given in mV and are presented as mean ± SEM. V_{50}, half maximal voltage of activation; k_{act}, steepness of activation curve

	V_{50}	k_{act}	n
15 Ca^{2+}	-4.7 ± 0.6	8.9 ± 0.3	21
15 Ba^{2+}	-18.3 ± 0.7	6.7 ± 0.5	13
15 Ca^{2+} +BayK	13.9 ± 0.9	6.2 ± 0.9	9

3.2. THE $CA_V1.4$ L216R (LR) MUTANT – LOSS OF FUNCTION

The LR mutation is located in transmembrane segment 4 of domain I, which forms part of the voltage sensor (Fig. 9).

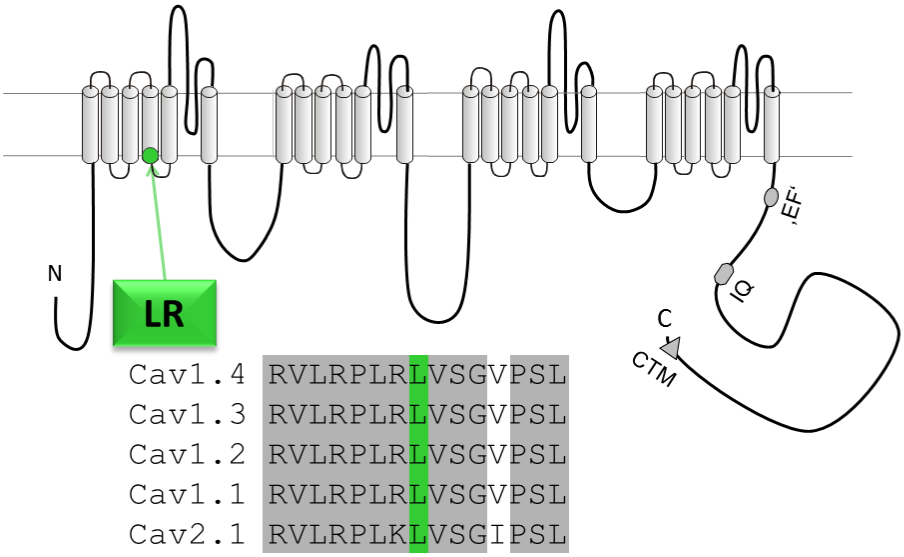

Figure 9: Localization of the L216R (LR) mutation in the α1 subunit of the Cav1.4 channel and sequence alignment of the respective region. The mutated leucine (highlighted in green) appears to be highly conserved among calcium channels.

Cells were held at a potential of -98 mV and depolarized from -78 mV up to +52 mV in 10 mV increments for 50 ms. The respective pulse protocol is shown in Fig. 10a. We did not observe any calcium currents through LR channels using 15 mM calcium or barium as charge carrier (Fig 10 b, c). Also after application of 3 µM of the calcium channel activator BayK, I could not elicit any current (Fig. 10d). In order to investigate whether LR channels mediated any currents (and to discriminate them from endogenous currents also found in mock-transfected cells), I analysed the maximum current density of each cell. Fig. 10 (e, f) shows that the maximal current densities of the LR channel are in the range of mock-transfected cells.

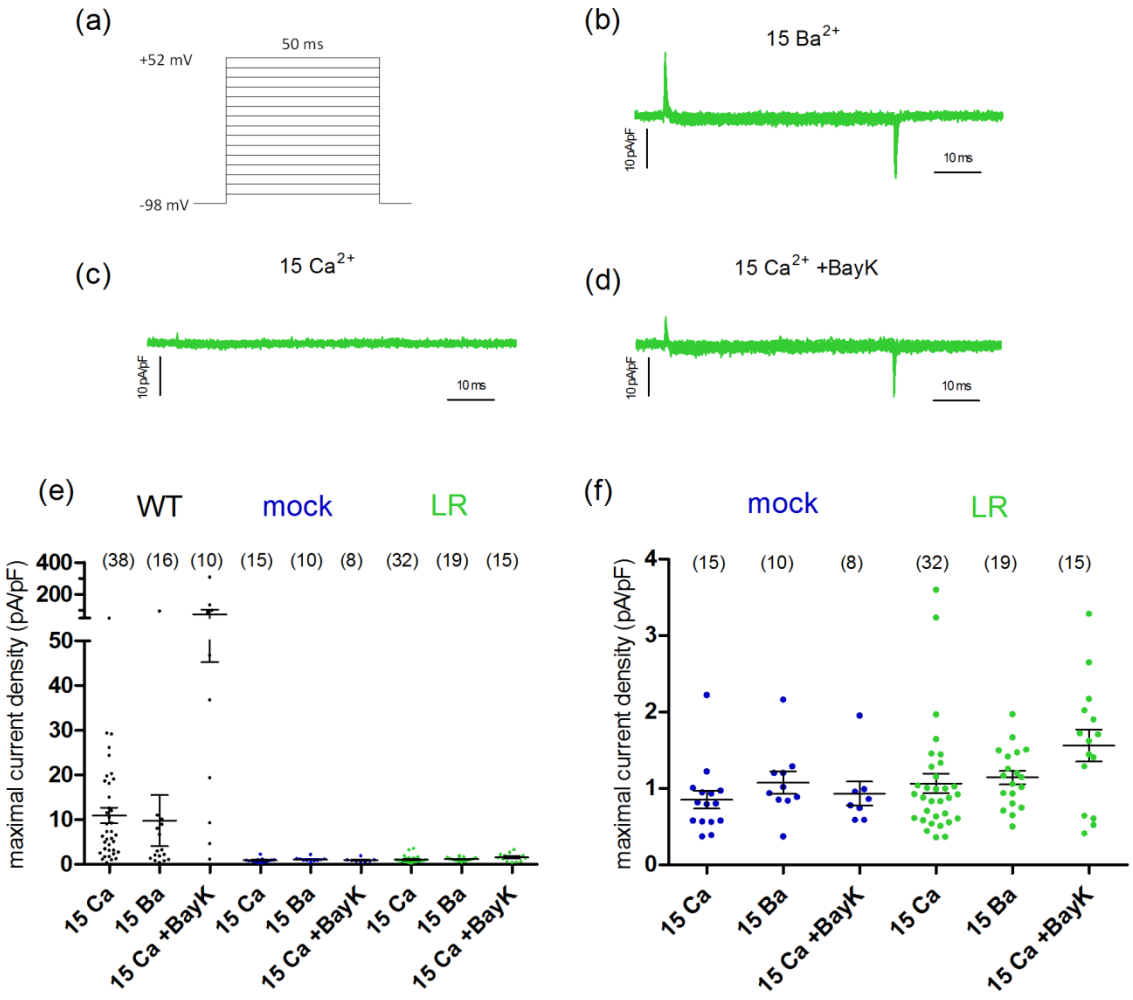

Figure 10. Representative currents and maximum current densities of mutant LR channels. (a) Pulse protocol. (b, c, d) representative currents mediated by LR channels transiently expressed in tsA-201 cells together with β_3 and $\alpha_2\delta$-1 subunits. The respective charge carriers are indicated. Traces do not represent the same cell. (e, f) maximal current densities of LR channels compared to WT and mock-transfected cells. Panel f shows the same mock and LR data points as panel e, but in a different scale. The bars represent the mean ± SEM. Numbers of experiments are given in parentheses.

There are at least three possible explanations for this observation:

(I) The number of channels expressed in the plasma membrane is reduced.

(II) Defective protein is not folded properly and therefore degraded.

(III) The LR channels cannot conduct calcium properly.

To address possibility I, we decided to check for gating currents of the LR channels because occurrence of gating currents would directly confirm the presence of channels at the cell surface. Gating currents reflect movement of the so-called voltage sensor upon depolarisation. The voltage sensor is positively charged due to the presence of arginine residues. Its movement induces opening of the channel pore and the charge movement can be detected as gating current at the beginning (ON gating current) and end (OFF gating current) of a pulse. Gating currents are characterised by their sigmoidal voltage dependence and are therefore discriminated from capacitive artefacts, which show

linear voltage dependence. Indeed, we observed gating currents in a minority of cells (3 cells out of 37) (Fig. 11).

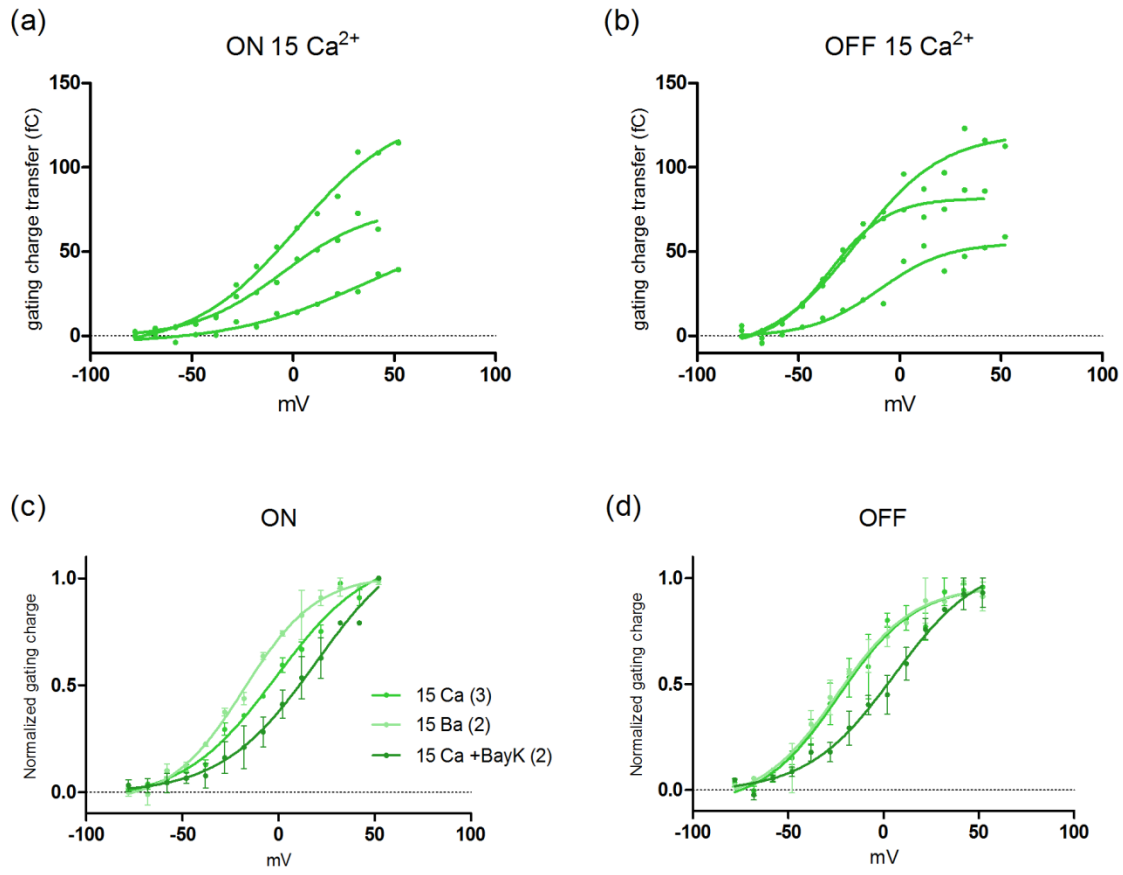

Figure 11. Voltage dependence of LR gating currents. Cells were clamped to -98mV and depolarised for 50ms from -78mV up to -52mV in 10mV increments. (a, b) ON and OFF gating currents in 15mM Ca for individual cells. (c,d) Normalized ON and OFF gating currents with different charge carriers indicated. Colour code is the same for d and d. Data are shown as means ± SEM. Numbers of experiments are given in parentheses.

When analysing gating currents, it is necessary to block the ion conductance to ensure that the gating current is not superimposed by the current of the ion flow. Although the LR mutant did, if at all, show only very little ionic conductance (see Fig. 11 b-d), I used 15mM Mg^{2+} as charge carrier and 15µM $GdCl_3$ in order to block any residual current; and compared LR with WT gating currents recorded under the same experimental conditions. For that purpose, the cell was clamped to -98 mV and depolarized from -78 mV up to +62 mV in 10 mV increments for 20 ms.

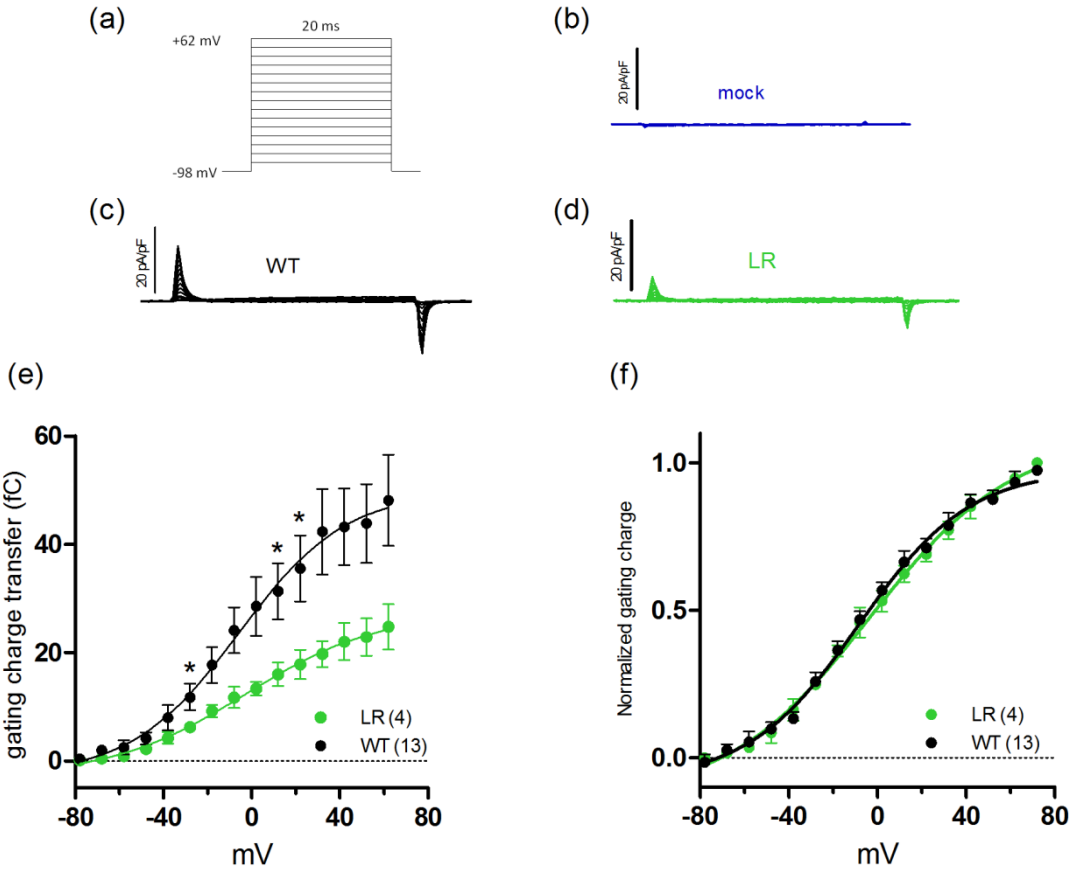

Figure 12. ON gating current properties of LR and WT channels. Currents were recorded using 15 mM Mg^{2+} as charge carrier supplemented with 15 µM $GdCl_3$. (a) Gating pulse protocol. Cells were held at -98 mV and depolarized for 20 ms from -78 mV up to 62 mV in 10 mV increments. (b, c, d) representative currents of tsA-201 cells transiently transfected with either no (mock, b), WT (c) or LR (d) channels together with β3 and α2δ-1 subunits. (e) Integrated gating currents (charge transfer) of WT and LR channels, both showing typical sigmoidal voltage dependence. (f) Normalized gating charge of WT and LR channels. Data are presented as mean ± SEM and numbers of experiments are given in parentheses. 7 of the wild type datasets depicted in (e) and (f) are courtesy of Verena Burtscher. *, $p<0.05$; Mann Whitney U-test

Under these conditions, 4 out of 25 cells transiently transfected with LR channels exhibited gating current. Figure 12 (c, d) illustrates the absence of any inward current as well as clearly defined gating current for wild type and LR. LR gating currents are considerably smaller than in wild type, but they show the same voltage dependence. Gating currents were clearly absent in mock-transfected cells which I used as negative control.

These data imply a reduction of channels expressed at the plasma membrane. We suggested that this finding should also be reflected in low expression of the channel on the protein level in transfected tsA-201 cells. However, we could previously show that LR channels were expressed at a similar level as wild type (by western blot, data not shown). Thus, we hypothesised that the LR channel may be subject to a faster turnover rate than wild type, leading to a reduced channel number at the cell surface. In order to address the turnover of $Ca_v1.4$ wild type and mutant channels, we performed a cycloheximide (CHX) chase experiment. The procedure of the experiment is outlined in Fig. 13.

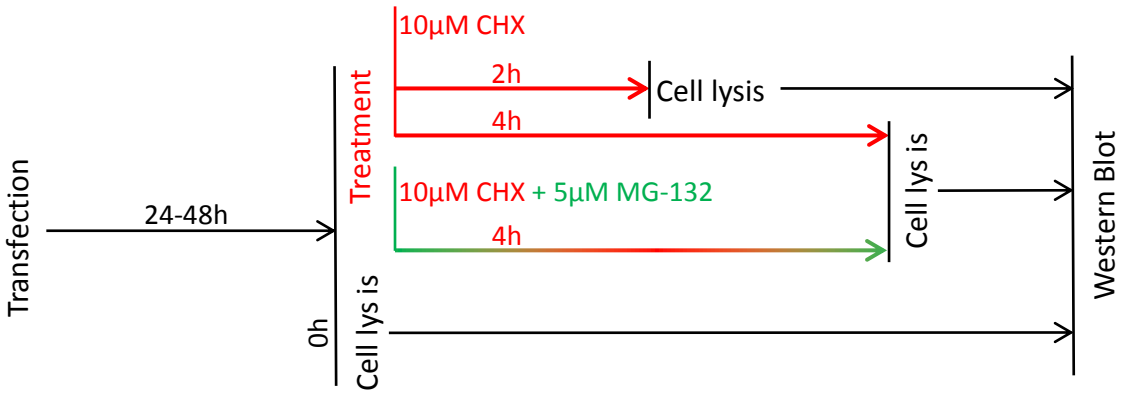

Figure 13. Cell treatment protocol used for determining the turnover of $Ca_v1.4$ channels (CHX chase experiment). CHX Cycloheximide; MG-132, cell permeable proteasomal inhibitor.

Cycloheximide blocks elongation and therefore inhibits protein synthesis (Schneider-Poetsch *et al.*, 2010). Therefore, degradation of the existing protein can be monitored over time. MG-132 treatment inhibits protein degradation via the proteasome. As a result, proteins are only degraded via lysosomal degradation pathways.

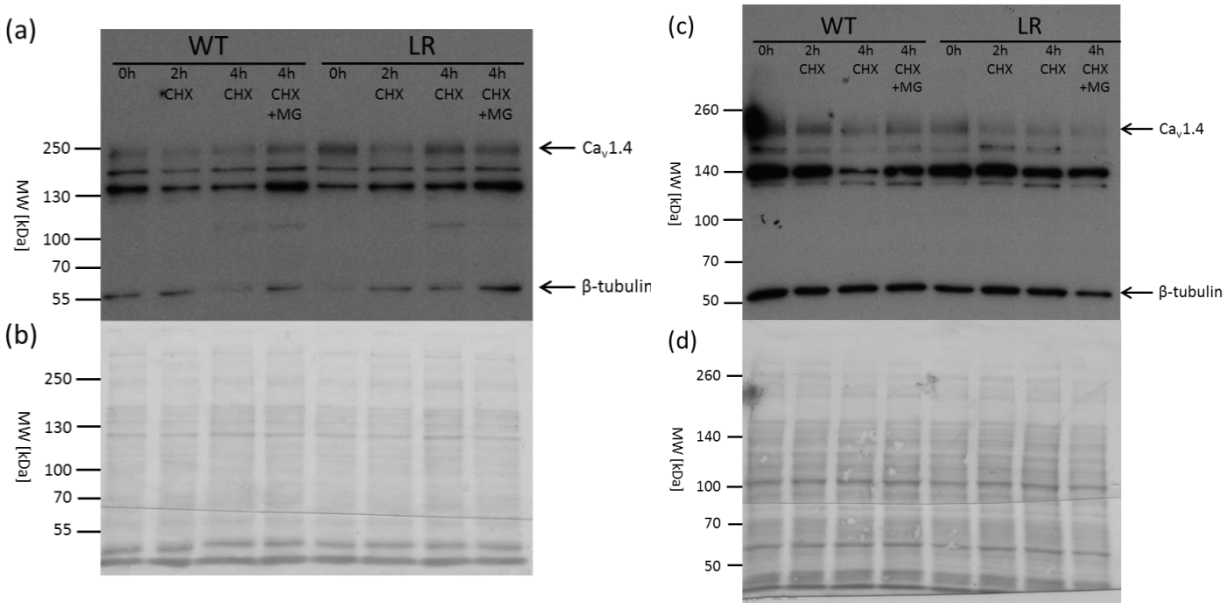

Figure 14. Degradation of WT and LR channels. Total protein was prepared from transfected tsA-201 cells (a, c) Western blot for $Ca_v1.4$ and β-tubulin (as a loading control). (b, d) Ponceau S staining of the membrane.

Two of my Western blot experiments and Ponceau S stainings are displayed in Fig. 14. I also stained the nitrocellulose membrane with Ponceau S to check if protein was homogenously loaded and transferred. Protein degradation was quantified as ratio of the level at 0h. Initially, beta-tubulin was chosen as loading control, but this turned out to be not constant (see also Fig. 14 a, c). I therefore corrected for the Ponceau S staining intensity of the respective lane. This procedure was previously

suggested to work better than any other housekeeping protein, since the latter potentially also are degraded (Romero-Calvo *et al.*, 2010).

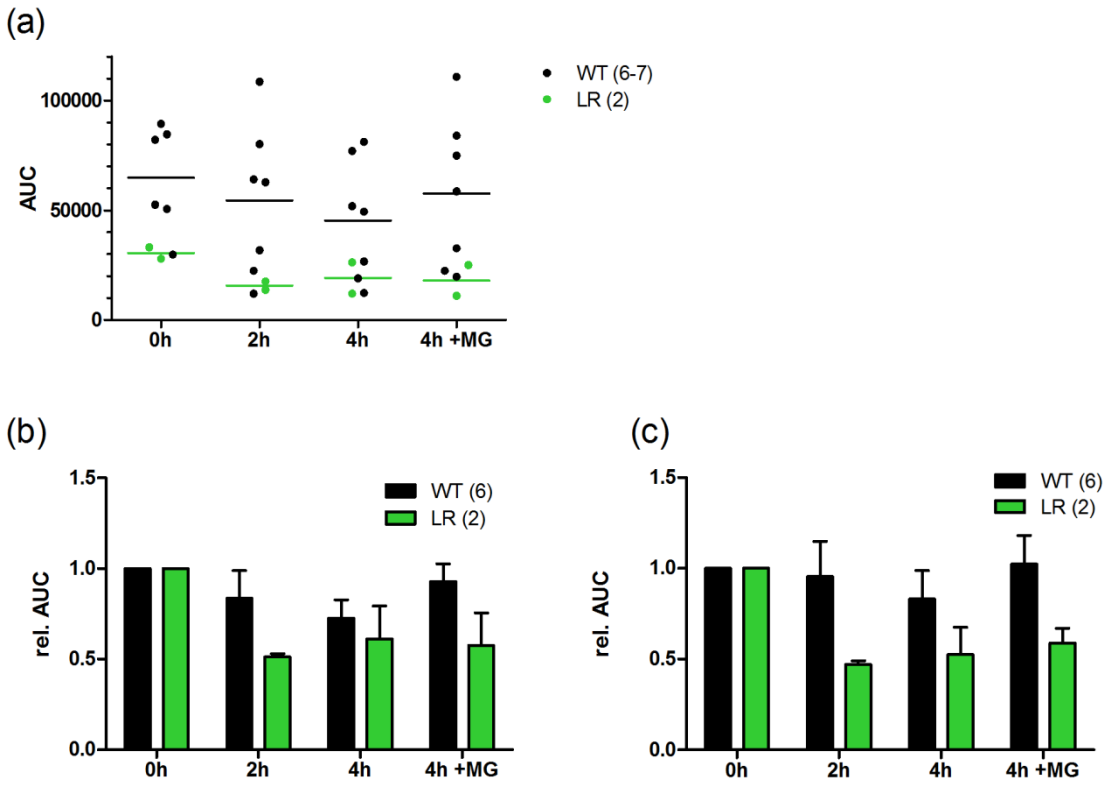

Figure 15. Quantification of CHX chase experiments. Immunostaining intensity of the $Ca_v1.4$ band was determined using ImageJ (Area under the curve). (a) absolute area under the curve of the specific $Ca_v1.4$ peak. (b) Same data as in (a), but normalized to 0h. (c) Same data again, but normalized to the Ponceau S staining of the respective lane. Data are expressed as mean ± SEM. 4 of the WT datasets are courtesy of Verena Burtscher.

As shown in Fig. 15, the levels of $Ca_v1.4$ WT protein remained fairly constant upon treatment with CHX. In contrast, levels of the $Ca_v1.4$ LR channel were already decreased after 2h in both experiments. Due to the low number of experiments (n=2 for LR), we cannot yet tell if this difference is statistically significant. However, my preliminary data point towards a faster turnover rate for LR channels, indicating reduced protein stability. Nonetheless, it has to be noted that our membrane preparation does not distinguish between plasma membrane and the bulk of endoplasmic reticulum membranes. Protein detected via this procedure may reside within the endoplasmic reticulum and is thus not capable of mediating calcium currents in our recordings.

I conclude from these experiments that a certain fraction of LR channels can be transported to the plasma membrane and their voltage sensor is functionally moving upon depolarization of the cell membrane. The strong reduction of calcium influx, however, indicates that the substitution of leucine by arginine might impair the link between the voltage sensor and the channel pore. In addition, LR channels might be improperly folded channels which undergo increased degradation in the cell. We have not yet investigated the single channel properties of LR channels which might add an additional aspect (e.g. due to a lower open probability).

3.3. THE $CA_V1.4$ R1827X (RX) MUTANT – C-TERMINAL TRUNCATION

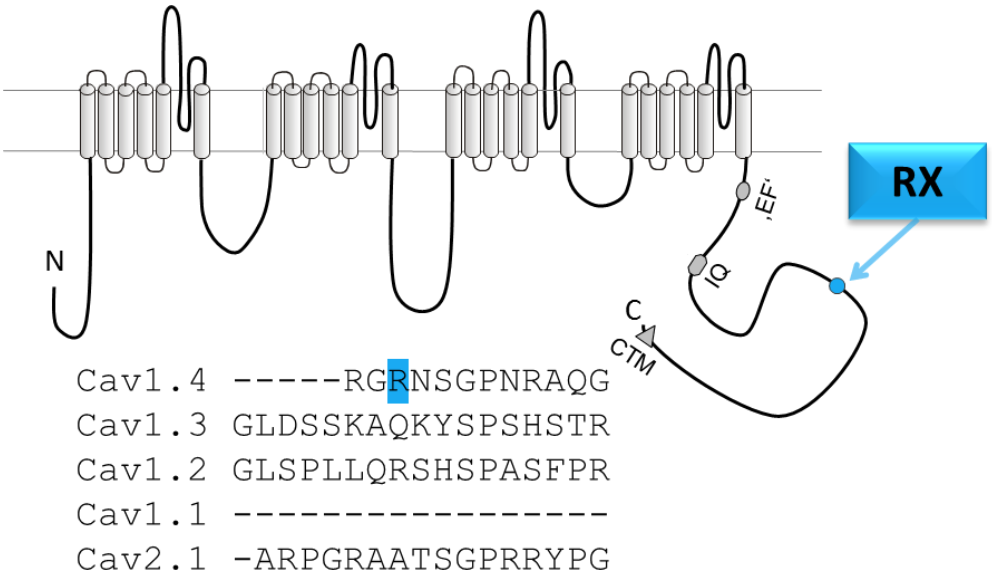

Figure 16. Localisation of the RX mutation in the Cav1.4 channel

Structurally, the RX mutation causes a truncation of the C-terminus (Fig. 16). I have tested the functional properties of RX channels by holding the cells at a potential of -98 mV and depolarizing them in 10 mV increments up to +52 mV for 300 ms. Sample traces using 15 mM Ca^{2+} and 15 mM Ba^{2+} are shown in Fig. 17 a. Inactivation is much more pronounced in I_{Ca} than in I_{Ba}, indicating CDI (Fig. 17a). I quantified CDI by the current remaining after 250 ms of depolarization expressed as a fraction of the peak current (r_{250}) (Fig. 17d). The lack of CTM not only leads to CDI in RX channels, but also causes a -12mV leftward shift in the voltage dependence of activation (Fig. 17, Tab. 20).

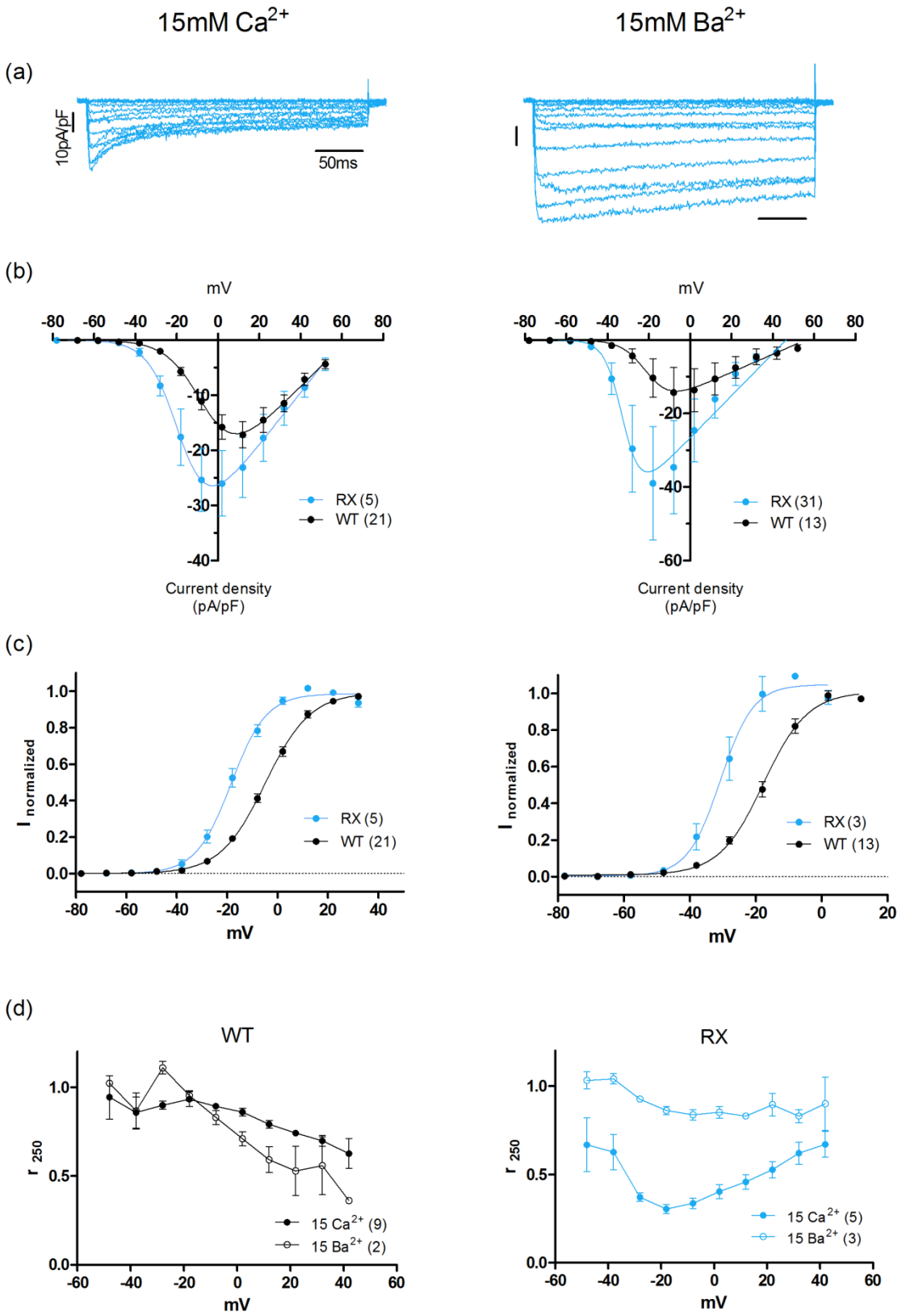

Figure 17. Representative currents and current-voltage relationships of $Ca_v1.4$ RX channels. (a) Representative sample traces of RX channels using 15 mM Ca^{2+} (left panel) or 15 mM Ba^{2+} (right panel). (b) Current densities of RX (light blue) compared to WT (black) channels in 15 mM Ca^{2+} (left) or 15 mM Ba^{2+} (right). (c) Activation properties of RX (light blue) and WT (black) channels. (d) Quantification of CDI by expressing the current after 250ms of depolarisation as a fraction of the peak current at the indicated potentials (r_{250} values) in WT and RX channels for 15 mM Ca^{2+} (filled circles) or 15 mM Ba^{2+} (open circles). Data are presented as mean ± SEM and numbers of experiments are indicated in parentheses.

Singh and colleges (2006) have characterised the truncation mutants K1591X and $Ca_v1.4_{\Delta C122}$ (deletion of the last 122 amino acids), which both also displayed CDI and a leftward shift in voltage-dependent activation. Co-expression with the last 122 amino acids of $Ca_v1.4$ (C122) rescued the phenotype of $Ca_v1.4_{\Delta C122}$ and slowed inactivation in K1591X, demonstrating that these 122 amino acids are responsible for the inhibition of CDI in $Ca_v1.4$ WT channels. However, the only partial recovery of K1591X indicates that the postIQ region is involved in the inhibition of CDI.

Thus, we hypothesised that co-expression of the C122 peptide will also rescue the RX phenotype by serving the missing CTM domain. Indeed, we showed that co-expression of C122 can restore $Ca_v1.4$ WT properties by both abolishing CDI and shifting voltage-dependent activation to the range of the WT channel (Fig. 19b). In addition to the deletion of the last 122 amino acids, also deletion of the last 55 amino acids of $Ca_v1.4$ caused CDI and a leftward shift in activation. In contrast, none of these effects was observed when the last 32 amino acids were missing. These results led to the hypothesis that the sequence of amino acids 1911-1934 is the determining sequence for CDI inhibition. The functional domains of the $Ca_v1.4$ C-terminus are displayed in Fig. 18.

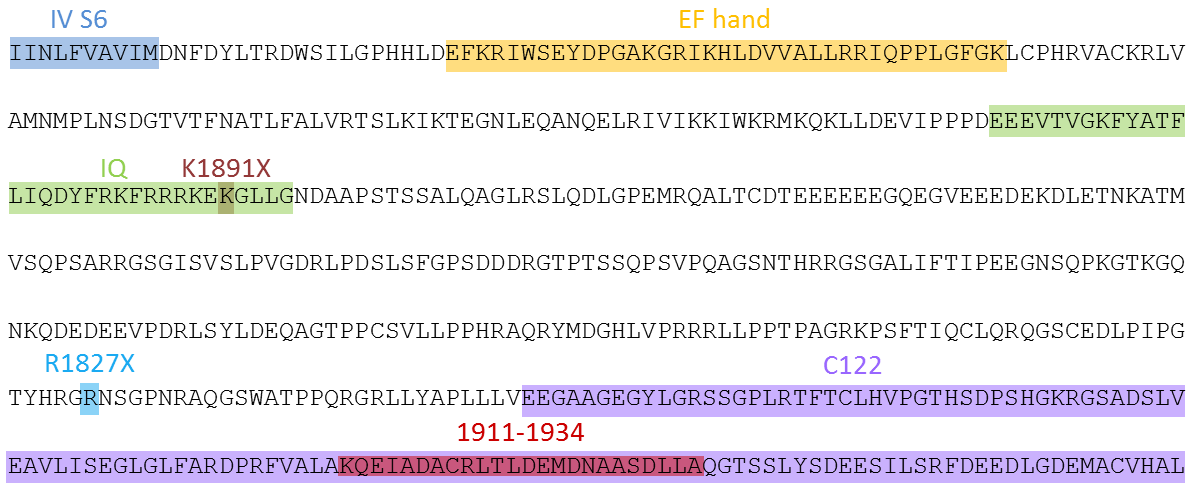

Figure 18. C-terminus of $Ca_v1.4$ and its functional domains.

I therefore wanted to test whether providing the shorter 1911-1934 peptide was sufficient for a rescue. To investigate this question I used an eGFP-tagged shorter peptide comprising the amino acid residues 1911-1934. Surprisingly, this did not alter RX gating properties (Fig. 19). This finding might be explained by the fact that the eGFP-tag sterically hinders the interaction between the short C-terminal sequence and the RX channel protein. Future investigations will involve an IRES-eGFP construct to follow up this question.

Tab. 20 summarizes the biophysical parameters of RX channels and their changes upon coexpression of C-terminal peptides.

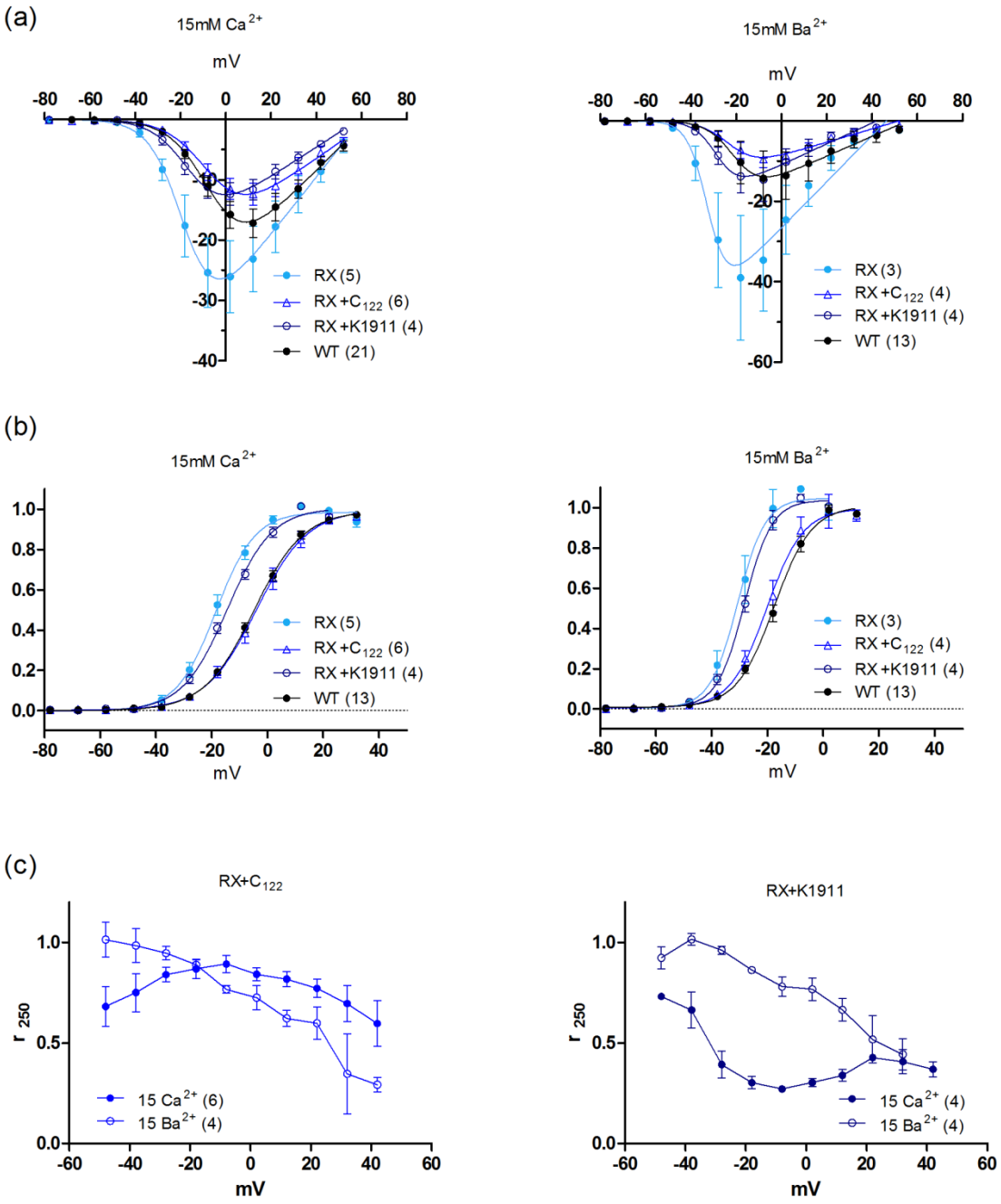

Figure 19. Biophysical properties of the RX channel coexpressed with C-terminal peptides. (a) Current densities of RX (light blue), WT (black), RX coexpressed with C122 (blue triangles) and RX coeypressed with the K1911 peptide (dark blue open circles) for the charge carriers indicated. (b) Activation properties of the channels in (a). Note the leftward shift in activation of RX channels, that is rescued by coexpression of C122, but not K1911. (c) r250 values of RX channels with coexpressed C-terminal peptides. C122 but not K1911 abolished CDI in RX channels.

Table 20. Biophysical parameters of WT and RX channels coexpressed with C-terminal peptides using different charge carriers. V_{50} , half maximal voltage of activation; k_{act} , steepness of activation curve. Data are all given in mV and are presented as mean ± SEM.

	15 Ca		15 Ba	
	V_{50}	k_{act}	V_{50}	k_{act}
WT	-4.7 ± 0.6	8.9 ± 0.3	-18.3 ± 0.7	6.7 ± 0.5
RX	-16.8 ± 0.9	7.5 ± 0.5	-31.4 ± 1.2	4.7 ± 0.9
RX + C122	-4.9 ± 1.0	9.1 ± 0.5	-20.7 ± 1	6.6 ± 0.7
RX +K1911	-14.4 ± 0.6	8.0 ± 0.4	-28.9 ± 0.6	4.9 ± 0.5

Taken together, these data reflect a complex dysfunction profile, as this phenotype combines loss-of-function (CDI) and gain-of-function (leftward shift in activation) properties. It remains elusive which of these functional impairments is also physiologically relevant and whether the net effect of the RX mutation is a loss-of-function or a gain-of-function phenotype.

3.4. THE $Ca_V1.4$ I745T (IT) MUTANT – GAIN OF FUNCTION

The IT missense mutation is located in the transmembrane segment 6 of domain II (Fig. 20). The exchange of a hydrophobic Isoleucine to a polar Threonine in a highly conserved region dramatically alters the gating properties of the channel. It has previously been reported to cause a leftward shift in the voltage dependance of activation of -34 mV (Hemara-Wahanui *et al.*, 2005; Hope *et al.*, 2005).

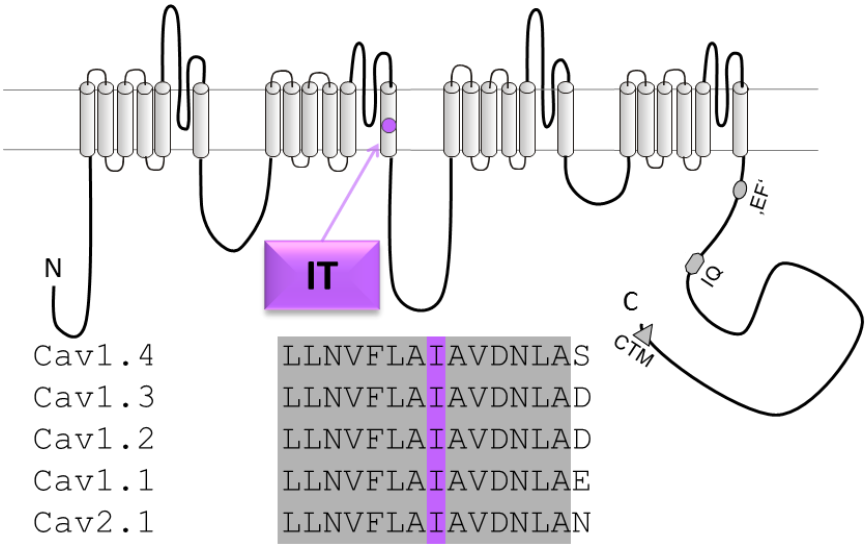

Figure 20. Localisation of the IT mutation in $Ca_V1.4$ and sequence alignment. The mutated isoleucine and its adjacent amino acids are highly conserved.

Cells were clamped to -98 mV and depolarized in 10mV increments up to +52mV for 50ms with 15 mM Ca^{2+} as charge carrier. Representative sample traces and the corresponding IV-curves and activation curves are shown in Fig. 21. Current-voltage relationships revealed a dramatic leftward shift by -37 mV compared to WT in 15 mM Ca^{2+}. In addition, the characteristic -10 mV shift caused by BayK in WT was diminished in the IT mutant (shift for WT -9.2 mV and IT +1.9 mV). Values of activation parameters are depicted in Tab. 21. This hyperpolarizing shift causes enhanced entry of Ca^{2+} and a gain-of-function of the channel. These results are in excellent correspondence with the work of (Hemara-Wahanui *et al.*, 2005), who reported a -34 mV leftward shift in activation.

Table 21. Biophysical parameters of WT and IT channels using different charge carriers. V_{50} , half maximal voltage of activation; k_{act} , steepness of activation curve. Data are given in mV and are presented as mean ± SEM.

	15mM Ca^{2+}		15mM Ca^{2+} +BayK	
	V_{50}	k_{act}	V_{50}	k_{act}
WT	-4.7 ± 0.6	8.9 ± 0.3	-13.9 ± 0.9	6.2 ± 0.9
IT	-41.6 ± 0.7	6.3 ± 0.5	-39.7 ± 0.4	4.7 ± 0.4

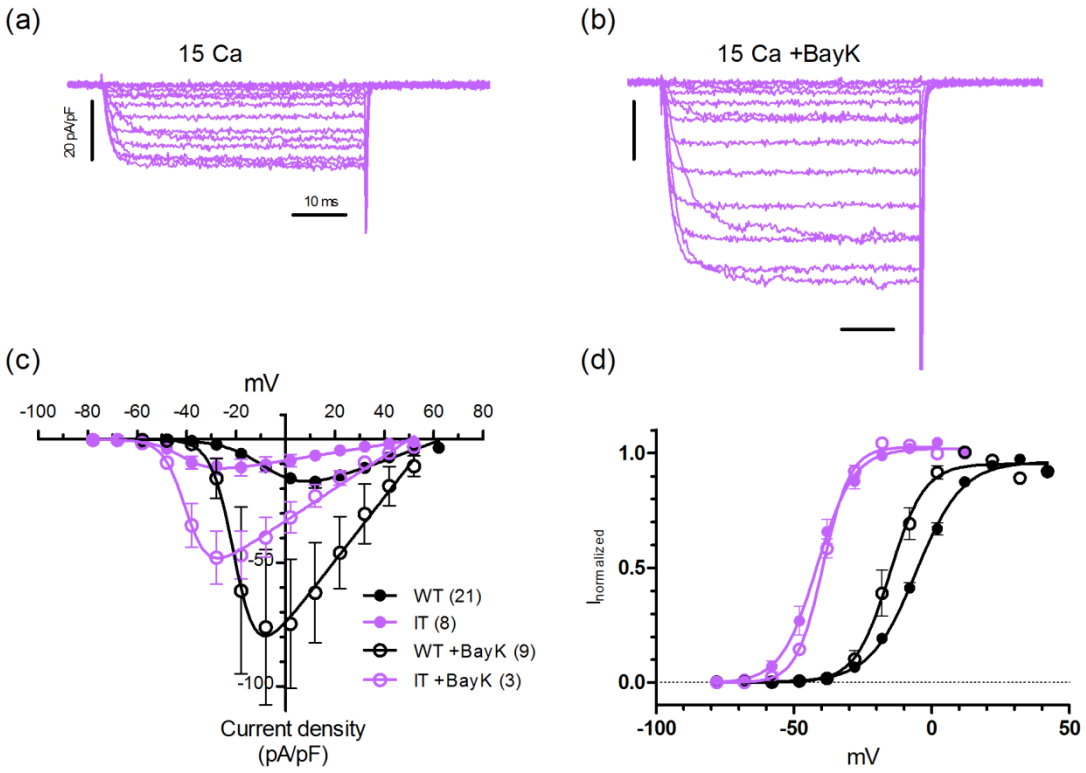

Figure 21. Representative currents and current-voltage relationships of Cav1.4 WT and mutant IT channels. (a, b) representative currents mediated by IT channels transiently expressed in tsA-201 cells together with β3 and α2δ-1 subunits for the charge carrier indicated. (c) Current densities for WT (black) and IT (purple) using 15mM Ca^{2+} (filled circles) or 15mM Ca^{2+} +3µM BayK (open circles) as charge carrier. (d) Voltage-dependent activation. Colour code is as in (c). Data are presented as means ± SEM for the indicated number of experiments.

In order to investigate the RX and IT mutant channels under more physiologically relevant conditions, I applied 20 ms depolarizing pulses to -20 mV from a holding potential of -70 mV at frequencies of 1, 2 and 5 Hz (Fig. 22a). This protocol was designed to mimic illumination (-70 mV) with short periods of darkness (-20 mV). We had to add 3 µM BayK in order to obtain currents of sufficient amplitude. Whereas the charge transfer was constant in WT and IT at all tested frequencies, we observed a decrease in RX channels at 2 Hz and 5 Hz starting with the second pulse. It is therefore plausible that RX channels are not capable of maintaining continuous calcium influx during illumination changes which is normally sustained by the non-inactivating nature of $Ca_v1.4$ channels.

Whereas both the RX and the IT mutant show a leftward shift in activation, CDI is only found in RX channels. We therefore suggest that frequency-dependent inactivation in RX is likely to be due to CDI. In addition, we conclude from this experiment that the loss of function (i.e. CDI) is the predominant factor contributing to the impairment of RX channel functionality. Accordingly, the RX mutant is likely to exhibit rather a loss-of-function than a gain-of-function phenotype under physiological conditions.

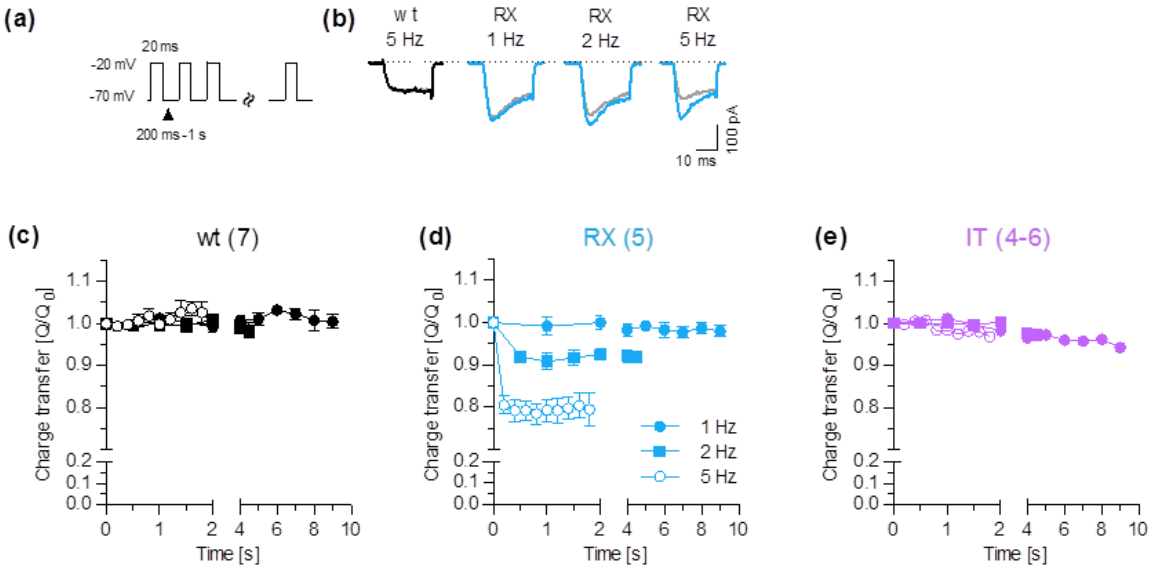

Figure 22. Frequency-dependent inactivation in WT, RX and IT channels. (a) pulse protocol. 20ms pulses to -20mV were applied at frequencies of 1, 2 and 5 Hz. (b) Representative traces for WT and RX at different frequencies. Black/light blue traces represent the first, grey the second pulse of the train. 15 mM Ca^{2+} + 3 µM BayK was used as charge carrier. (c, d, e) Charge transfer of WT, RX and IT channels normalized to the first pulse. Data are depicted as mean ± SEM for the indicated number of experiments.

4. DISCUSSION

Defective retinal synaptic transmission in patients affected with congenital stationary night blindness type 2 (CSNB2) can result from different dysfunction phenotypes in $Ca_v1.4$ L-type calcium channels. Here, I investigated three different prototypical $Ca_v1.4$ variants representing this functional spectrum and analysed their biophysical properties via whole-cell patch clamp technique.

The $Ca_v1.4$ LR mutation has previously been identified in a patient suffering from CSNB2 (Christina Zeitz, unpublished) and resides within the transmembrane segment 4 of domain 1, which forms part of the voltage sensor. The voltage sensor is positively charged due to the presence of arginine residues and can therefore move upon voltage changes and drives the conformational change leading to the opening of the channel (Bezanilla, 2008; Swartz, 2008). The replacement of the leucine for an arginine residue in LR channels introduces an additional positive charge and leads to a loss-of-function phenotype.

Western Blot experiments showed that protein expression levels of LR channels are comparable to WT channels. However, our membrane preparation does not distinguish between plasma membrane and other membranous cell compartments. Therefore, the lack of calcium influx in LR channels could be either explained by non-functional channels at the plasma membrane or by absence or severe reduction in channel number at the cell surface. This could be due to a folding problem of mutant channels enhancing protein degradation. The occurrence of gating currents confirms the presence of (at least some) LR channels at the plasma membrane. In addition, our CHX experiments showed a trend towards faster protein turnover in LR channels. Taken together, these results indicate that this loss-of-function phenotype is likely to be caused by a combination of both mechanisms.

Recently, our working group described another $Ca_v1.4$ mutation leading to a loss-of-function, namely L860P (Burtscher *et al.*, 2014). In contrast to LR channels, this mutant showed reduced, but detectable calcium influx due to a reduced number of functionally active channels without gross changes in gating properties. Interestingly, no gating currents could be detected. Thus, we speculate that the loss-of-function phenotype of LR channels is more likely to be caused by a non-functionality of the single channels rather than by a reduction in channel number. In particular, the smaller gating currents in LR channels could be due to a reduction of movement of the voltage sensor, which prevents functional coupling of the voltage sensor with opening of the pore, thus hampering calcium influx.

In close proximity to the LR substitution, another loss-of-function mutation in $Ca_v1.4$ (S229P) is situated in the S4-S5 linker (Hoda *et al.*, 2006). In their study, the authors could not detect barium currents using *Xenopus* oocytes as expression system, but showed that the protein was expressed (via western blot); suggesting that either targeting of the channels was prevented or channel gating was obstructed. Given the close proximity and similar phenotype, LR and S229P mutations might interfere with channel gating via similar mechanisms. It was suggested that the insertion of the polar

proline in S229P might impair mechanical communication of the voltage sensor via the S4-S5 linker helix due to its helix breaking properties or an increase in hydrophobicity, thus stabilizing the closed state of the channel (Stockner & Koschak, 2013). Intriguingly, the S229P mutation in $Ca_v1.4$ aligns with S218L in $Ca_v2.1$, which has been shown to be linked to a severe form of familial hemiplegic migraine with delayed cerebral oedema and coma after minor head trauma (Kors *et al.*, 2001). These data implicate that the S4-S5 domains serve as a 'gating hot spot' in voltage-gated calcium channels.

As the functional consequence of the LR mutation is a complete loss of calcium influx, its physiological outcome is expected to be comparable to that of a $Ca_v1.4$ KO. $Ca_v1.4$ KO mice have defects in ribbon synapse development (Liu *et al.*, 2013; Zabouri & Haverkamp, 2013), suggesting that proper $Ca_v1.4$ functionality is required for the maturation of ribbon synapses.

The analysis of $Ca_v1.4$ truncation mutants has previously led to the discovery of the CTM that modulates gating (Singh *et al.*, 2006; Wahl-Schott *et al.*, 2006). As the RX channel is characterised by both a leftward shift in activation and calcium dependent inactivation, it is difficult to predict the physiological effect of the mutation. The hyperpolarising shift in the voltage dependence of activation is predicted to reduce the dynamic range of the photoreceptor, thus changing synaptic transmission. The occurrence of inactivation at potentials relevant for photoreceptor signalling is likely to further decrease the dynamic range. A mouse model with a truncated $Ca_v1.4$ to test these suggestions in whole-mount retinas or *in vivo* is not yet available, but will help to elucidate this issue. However, our data on frequency-dependent inactivation data in RX and IT channels suggest that the loss-of-function phenotype is predominant under physiological conditions.

We aimed to rescue the RX phenotype by coexpression of a short C-terminal peptide as suggested by previous studies (Singh *et al.*, 2006). However, we could not observe any changes in gating properties. This might be explained by steric hindrance of the big eGFP tag, thus hindering proper interaction of the peptide with its target. Future studies will further elucidate this issue by using an IRES-construct, thus avoiding direct tagging of the peptide.

The point mutation IT has been described in a New Zealand family, in which affected members show a phenotype similar to CSNB2. However, some patients show additional intellectual impairment or autism. Additionally, also female heterozygotes are affected in a similar, but in a less severe way than their male family members (Hemara-Wahanui *et al.*, 2005; Hope *et al.*, 2005). We (my master thesis) and others (Hemara-Wahanui et al., 2005) found a dramatic leftward shift (-34mV) in the voltage dependence of channel activation, indicating that this mutation leads to a gain-of-function of $Ca_v1.4$.

The exchange of the hydrophobic isoleucine to a polar threonine is suggested to increase the open probability by destabilizing the closed confirmation, as threonine cannot form a stable interaction with the adjacent S6 and the S4-S5 linker (Stockner & Koschak, 2013). Physiologically, the shift in activation to more hyperpolarised potentials enhances calcium influx during illumination, but reduces the increase in calcium influx upon depolarisation. Thus, this gain-of-function reduces the dynamic range of the photoreceptor, which then causes a change in glutamate release and thereby reduces synaptic transmission. Alternatively, the increased calcium influx might trigger cell death and lead to

an overall loss-of-function effect. Photoreceptors have a membrane potential around -55mV (in light conditions). At this potential, wild type $Ca_v1.4$ is closed, whereas the IT channel is already open, causing continuing calcium influx. The hypothesis of calcium-triggered cell death is further strengthened by the fact that I had to use calcium-free medium for the expression of the IT channels, as tsA-201 cells would rarely express the IT channel or die in presence of calcium. Morphological analysis of mice carrying the IT channel revealed thinner outer nuclear layers and shorter cone outer segments. In addition, the organization of the outer plexiform layer was disrupted and ribbon synapses appeared abnormal (Knoflach *et al.*, 2013).

Taken together, these findings indicate the wide spectrum of $Ca_v1.4$ mutations found in CSNB2 patients, which has to be considered for future therapeutic approaches. Pharmacological intervention via calcium-channel blockers such as dihydropyridines might not serve as a good option, as these substances are not clearly LTCC subtype-selective and therefore cardiac side effects are expected. It is rather favourable to modulate $Ca_v1.4$ activity (e.g. via C-terminal modulation in RX channels). However, data from $Ca_v1.4$ KO and $Ca_v1.4^{I745T}$ knock-in mice indicate that there are developmental changes in the retina which will require early therapeutic intervention.

5. REFERENCES

Azizan, E.A.B., Poulsen, H., Tuluc, P., Zhou, J., Clausen, M. V, Lieb, A., Maniero, C., Garg, S., Bochukova, E.G., Zhao, W., Shaikh, L.H., Brighton, C.A., Teo, A.E.D., Davenport, A.P., Dekkers, T., Tops, B., Küsters, B., Ceral, J., Yeo, G.S.H., Neogi, S.G., McFarlane, I., Rosenfeld, N., Marass, F., Hadfield, J., Margas, W., Chaggar, K., Solar, M., Deinum, J., Dolphin, A.C., Farooqi, I.S., Striessnig, J., Nissen, P., & Brown, M.J. (2013) Somatic mutations in ATP1A1 and CACNA1D underlie a common subtype of adrenal hypertension. *Nat. Genet.*, **45**, 1055–1060.

Bading, H. (2013) Nuclear calcium signalling in the regulation of brain function. *Nat. Rev. Neurosci.*, **14**, 593–608.

Baig, S.M., Koschak, A., Lieb, A., Gebhart, M., Dafinger, C., Nürnberg, G., Ali, A., Ahmad, I., Sinnegger-Brauns, M.J., Brandt, N., Engel, J., Mangoni, M.E., Farooq, M., Khan, H.U., Nürnberg, P., Striessnig, J., & Bolz, H.J. (2011) Loss of Ca(v)1.3 (CACNA1D) function in a human channelopathy with bradycardia and congenital deafness. *Nat. Neurosci.*, **14**, 77–84.

Bauer, C.S., Tran-Van-Minh, A., Kadurin, I., & Dolphin, A.C. (2010) A new look at calcium channel α2δ subunits. *Curr. Opin. Neurobiol.*, **20**, 563–571.

Baumann, L., Gerstner, A., Zong, X., Biel, M., & Wahl-Schott, C. (2004) Functional Characterization of the L-type Ca2+ Channel Cav1.4α1 from Mouse Retina. *Investig. Ophthalmol. Vis. Sci.*, **45**, 708 –713.

Bech-Hansen, N.T., Naylor, M., Maybaum, T., Pearce, W., Koop, B., Fishman, G. a, Mets, M., Musarella, M. a, & Boycott, K. (1998) Loss-of-function mutations in a calcium-channel alpha1-subunit gene in Xp11.23 cause incomplete X-linked congenital stationary night blindness. *Nat. Genet.*, **19**, 264–267.

Bezanilla, F. (2008) How membrane proteins sense voltage. *Nat. Rev. Mol. Cell Biol.*, **9**, 323–332.

Boycott, K., Maybaum, T., Naylor, M., Weleber, R., Robitaille, J., Miyake, Y., Bergen, A., Pierpont, M., Pearce, W., & Bech-Hansen, N.T. (2001) A summary of 20 CACNA1F mutations identified in 36 families with incomplete X-linked congenital stationary night blindness, and characterization of splice variants. *Hum. Genet.*, **108**, 91–97.

Buraei, Z. & Yang, J. (2010) The ß subunit of voltage-gated Ca2+ channels. *Physiol. Rev.*, **90**, 1461–1506.

Burtscher, V., Schicker, K., Novikova, E., Pöhn, B., Stockner, T., Kugler, C., Singh, A., Zeitz, C., Lancelot, M.-E., Audo, I., Leroy, B.P., Freissmuth, M., Herzig, S., Matthes, J., & Koschak, A. (2014) Spectrum of Cav1.4 dysfunction in congenital stationary night blindness type 2. *Biochim. Biophys. Acta*,.

Catterall, W. a, Perez-Reyes, E., Snutch, T.P., & Striessnig, J. (2005) International Union of Pharmacology. XLVIII. Nomenclature and structure-function relationships of voltage-gated calcium channels. *Pharmacol. Rev.*, **57**, 411–425.

Christel, C. & Lee, A. (2012) Ca2+-dependent modulation of voltage-gated Ca2+ channels. *Biochim. Biophys. Acta*, **1820**, 1243–1252.

Davies, A., Hendrich, J., Van Minh, A.T., Wratten, J., Douglas, L., & Dolphin, A.C. (2007) Functional biology of the alpha(2)delta subunits of voltage-gated calcium channels. *Trends Pharmacol. Sci.*, **28**, 220–228.

Doering, C.J., Hamid, J., Simms, B., McRory, J.E., & Zamponi, G.W. (2005) Cav1.4 encodes a calcium channel with low open probability and unitary conductance. *Biophys. J.*, **89**, 3042–3048.

Dolphin, A.C. (2003) Beta subunits of voltage-gated calcium channels. *J. Bioenerg. Biomembr.*, **35**, 599–620.

Dolphin, A.C. (2009) Calcium channel diversity: multiple roles of calcium channel subunits. *Curr. Opin. Neurobiol.*, **19**, 237–244.

Griessmeier, K., Cuny, H., Rötzer, K., Griesbeck, O., Harz, H., Biel, M., & Wahl-Schott, C. (2009) Calmodulin is a functional regulator of Cav1.4 L-type Ca2+ channels. *J. Biol. Chem.*, **284**, 29809–29816.

Hemara-Wahanui, A., Berjukow, S., Hope, C.I., Dearden, P.K., Wu, S.-B., Wilson-Wheeler, J., Sharp, D.M., Lundon-Treweek, P., Clover, G.M., Hoda, J.-C., Striessnig, J., Marksteiner, R., Hering, S., & Maw, M. a (2005) A CACNA1F mutation identified in an X-linked retinal disorder shifts the voltage dependence of Cav1.4 channel activation. *Proc. Natl. Acad. Sci. U. S. A.*, **102**, 7553–7558.

Hoda, J.-C., Zaghetto, F., Koschak, A., & Striessnig, J. (2005) Congenital stationary night blindness type 2 mutations S229P, G369D, L1068P, and W1440X alter channel gating or functional expression of Ca(v)1.4 L-type Ca2+ channels. *J. Neurosci.*, **25**, 252–259.

Hoda, J.-C., Zaghetto, F., Singh, A., Koschak, A., & Striessnig, J. (2006) Effects of congenital stationary night blindness type 2 mutations R508Q and L1364H on Cav1.4 L-type Ca2+ channel function and expression. *J. Neurochem.*, **96**, 1648–1658.

Hope, C.I., Sharp, D.M., Hemara-Wahanui, A., Sissingh, J.I., Lundon, P., Mitchell, E. a, Maw, M. a, & Clover, G.M. (2005) Clinical manifestations of a unique X-linked retinal disorder in a large New Zealand family with a novel mutation in CACNA1F, the gene responsible for CSNB2. *Clin. Exp. Ophthalmol.*, **33**, 129–136.

Jacobi, F.K., Hamel, C.P., Arnaud, B., Blin, N., Broghammer, M., Jacobi, P.C., Apfelstedt-Sylla, E., & Pusch, C.M. (2003) *A Novel CACNA1F Mutation in a French Family with the Incomplete Type of X-Linked Congenital Stationary Night Blindness.*, American Journal of Ophthalmology. Elsevier Inc.

Knoflach, D., Kerov, V., Sartori, S.B., Obermair, G.J., Schmuckermair, C., Liu, X., Sothilingam, V., Garrido, M.G., Baker, S.A., Glösmann, M., Schicker, K., Seeliger, M., Lee, A., & Koschak, A. (2013) Cav1.4 IT mouse as model for vision impairment in human congenital stationary night blindness type 2. *Channels (Austin).*, **7**.

Kors, E.E., Terwindt, G.M., Vermeulen, F.L., Fitzsimons, R.B., Jardine, P.E., Heywood, P., Love, S., van den Maagdenberg, A.M., Haan, J., Frants, R.R., & Ferrari, M.D. (2001) Delayed cerebral edema and fatal coma after minor head trauma: role of the CACNA1A calcium channel subunit gene and relationship with familial hemiplegic migraine. *Ann. Neurol.*, **49**, 753–760.

Koschak, A. (2010) Impact of gating modulation in CaV1.3 L-type calcium channels. *Channels (Austin).*, **4**, 523–525.

Koschak, A., Reimer, D., Walter, D., Hoda, J.-C., Heinzle, T., Grabner, M., & Striessnig, J. (2003) Cav1.4alpha1 subunits can form slowly inactivating dihydropyridine-sensitive L-type Ca2+ channels lacking Ca2+-dependent inactivation. *J. Neurosci.*, **23**, 6041–6049.

Liu, X., Kerov, V., Haeseleer, F., Majumder, A., Artemyev, N., Baker, S.A., & Lee, A. (2013) Dysregulation of Cav 1.4 channels disrupts the maturation of photoreceptor synaptic ribbons in congenital stationary night blindness type 2. *Channels (Austin).*, **7**.

Lowry, O.H., Rosebrough, N.J., Farr, A.L., & Randall, R.J. (1951) Protein measurement with the Folin phenol reagent. *J. Biol. Chem.*, **193**, 265–275.

Mansergh, F., Orton, N.C., Vessey, J.P., Lalonde, M.R., Stell, W.K., Tremblay, F., Barnes, S., Rancourt, D.E., & Bech-Hansen, N.T. (2005) Mutation of the calcium channel gene Cacna1f disrupts calcium signaling, synaptic transmission and cellular organization in mouse retina. *Hum. Mol. Genet.*, **14**, 3035–3046.

McRory, J.E., Hamid, J., Doering, C.J., Garcia, E., Parker, R., Hamming, K., Chen, L., Hildebrand, M., Beedle, A.M., Feldcamp, L., Zamponi, G.W., & Snutch, T.P. (2004) The CACNA1F gene encodes an L-type calcium channel with unique biophysical properties and tissue distribution. *J. Neurosci.*, **24**, 1707–1718.

Miyake, Y., Yagasaki, K., Horiguchi, M., Kawase, Y., & Kanda, T. (1986) Congenital stationary night blindness with negative electroretinogram. A new classification. *Arch. Ophthalmol.*, **104**, 1013–1020.

Morgans, C.W. (2001) Localization of the alpha(1F) calcium channel subunit in the rat retina. *Invest. Ophthalmol. Vis. Sci.*, **42**, 2414–2418.

Morgans, C.W., Bayley, P.R., Oesch, N.W., Ren, G., Akileswaran, L., & Taylor, W.R. (2005) Photoreceptor calcium channels: insight from night blindness. *Vis. Neurosci.*, **22**, 561–568.

Nakamura, M., Ito, S., Terasaki, H., & Miyake, Y. (2001) Novel CACNA1F Mutations in Japanese Patients with Incomplete Congenital Stationary Night Blindness. *Invest. Ophthalmol. Vis. Sci.*, **42**, 1610–1616.

Peloquin, J.B., Doering, C.J., Rehak, R., & McRory, J.E. (2008) Temperature dependence of Cav1.4 calcium channel gating. *Neuroscience*, **151**, 1066–1083.

Peloquin, J.B., Rehak, R., Doering, C.J., & McRory, J.E. (2007) Functional analysis of congenital stationary night blindness type-2 CACNA1F mutations F742C, G1007R, and R1049W. *Neuroscience*, **150**, 335–345.

Romero-Calvo, I., Ocón, B., Martínez-Moya, P., Suárez, M.D., Zarzuelo, A., Martínez-Augustin, O., & de Medina, F.S. (2010) Reversible Ponceau staining as a loading control alternative to actin in Western blots. *Anal. Biochem.*, **401**, 318–320.

Schneider-Poetsch, T., Ju, J., Eyler, D.E., Dang, Y., Bhat, S., Merrick, W.C., Green, R., Shen, B., & Liu, J.O. (2010) Inhibition of eukaryotic translation elongation by cycloheximide and lactimidomycin. *Nat. Chem. Biol.*, **6**, 209–217.

Schubert, G. & Bornschein, H. (1952) Analysis of the human electroretinogram. *Ophthalmologica.*, **123**, 396–413.

Shaltiel, L., Paparizos, C., Fenske, S., Hassan, S., Gruner, C., Rötzer, K., Biel, M., & Wahl-Schott, C. (2012) Complex regulation of voltage-dependent activation and inactivation properties of retinal voltage-gated Cav1.4 L-type Ca2+ channels by Ca2+-binding protein 4 (CaBP4). *J. Biol. Chem.*, **287**, 36312–36321.

Singh, A., Hamedinger, D., Hoda, J.-C., Gebhart, M., Koschak, A., Romanin, C., & Striessnig, J. (2006) C-terminal modulator controls Ca2+-dependent gating of Ca(v)1.4 L-type Ca2+ channels. *Nat. Neurosci.*, **9**, 1108–1116.

Splawski, I., Timothy, K.W., Decher, N., Kumar, P., Sachse, F.B., Beggs, A.H., Sanguinetti, M.C., & Keating, M.T. (2005) Severe arrhythmia disorder caused by cardiac L-type calcium channel mutations. *Proc. Natl. Acad. Sci. U. S. A.*, **102**, 8089–96; discussion 8086–8.

Stockner, T. & Koschak, A. (2013) What can naturally occurring mutations tell us about Ca(v)1.x channel function? *Biochim. Biophys. Acta*, **1828**, 1598–1607.

Striessnig, J., Bolz, H.J., & Koschak, A. (2010) Channelopathies in Cav1.1, Cav1.3, and Cav1.4 voltage-gated L-type Ca2+ channels. *Pflugers Arch.*, **460**, 361–374.

Strom, T.M., Nyakatura, G., Apfelstedt-sylla, E., Hellebrand, H., Lorenz, B., Weber, B.H.F., Wutz, K., Gutwillinger, N., Rüther, K., Drescher, B., Sauer, C., Zrenner, E., Meitinger, T., Rosenthal, A., & Meindl, A. (1998) An L-type calcium-channel gene mutated in incomplete X-linked congenital stationary night blindness. *Nat. Genet.*, **19**, 260–263.

Swartz, K.J. (2008) Sensing voltage across lipid membranes. *Nature*, **456**, 891–897.

Tan, G.M.Y., Yu, D., Wang, J., & Soong, T.W. (2012) Alternative splicing at C terminus of Ca(V)1.4 calcium channel modulates calcium-dependent inactivation, activation potential, and current density. *J. Biol. Chem.*, **287**, 832–847.

Wahl-Schott, C., Baumann, L., Cuny, H., Eckert, C., Griessmeier, K., & Biel, M. (2006) Switching off calcium-dependent inactivation in L-type calcium channels by an autoinhibitory domain. *Proc. Natl. Acad. Sci. U. S. A.*, **103**, 15657–15662.

Wässle, H. (2004) Parallel processing in the mammalian retina. *Nat. Rev. Neurosci.*, **5**, 747–757.

Wutz, K., Sauer, C., Zrenner, E., Lorenz, B., Alitalo, T., Broghammer, M., Hergersberg, M., de la Chapelle, A., Weber, B.H.F., Wissinger, B., Meindl, A., & Pusch, C.M. (2002) Thirty distinct CACNA1F mutations in 33 families with incomplete type of XLCSNB and Cacna1f expression profiling in mouse retina. *Eur. J. Hum. Genet.*, **10**, 449–456.

Zabouri, N. & Haverkamp, S. (2013) Calcium channel-dependent molecular maturation of photoreceptor synapses. *PLoS One*, **8**, e63853.

Zeitz, C., Labs, S., Lorenz, B., Forster, U., Uksti, J., Kroes, H.Y., De Baere, E., Leroy, B.P., Cremers, F.P.M., Wittmer, M., van Genderen, M.M., Sahel, J.-A., Audo, I., Poloschek, C.M., Mohand-Saïd, S., Fleischhauer, J.C., Hüffmeier, U., Moskova-Doumanova, V., Levin, A. V, Hamel, C.P., Leifert, D., Munier, F.L., Schorderet, D.F., Zrenner, E., Friedburg, C., Wissinger, B., Kohl, S., & Berger, W. (2009) Genotyping microarray for CSNB-associated genes. *Invest. Ophthalmol. Vis. Sci.*, **50**, 5919–5926.

Zeitz, C., Minotti, R., Feil, S., Mátyás, G., Cremers, F.P.M., Hoyng, C.B., & Berger, W. (2005) Novel mutations in CACNA1F and NYX in Dutch families with X-linked congenital stationary night blindness. *Mol. Vis.*, **11**, 179–183.

6. APPENDIX

6.1. ABSTRACT

The L-type calcium channel $Ca_v1.4$ is almost exclusively expressed in the retina, where it couples changes in illumination to glutamate release. Different dysfunction phenotypes of this channel have been shown to cause congenital stationary night blindness type 2 (CSNB2). In this study, I analysed three prototypical $Ca_v1.4$ mutations that were found in CSNB2 patients. I expressed these channels in tsA-201 cells and investigated their biophysical properties by whole-cell patch clamp technique.

The point mutation L216R (LR), which is located in the voltage sensor showed a loss-of-function phenotype, as no calcium influx could be detected. This could be either explained by a reduced number of channels on the cell membrane or by non-functional LR channels at the membrane. We observed gating currents in a minority of cells, indicating cell surface expression. In addition, we found a tendency towards increased protein degradation. Taken together, this phenotype is likely to be caused by a functional uncoupling of the voltage sensor movement and pore opening.

The truncation mutant R1827X (RX) lacks the C-terminal modulator domain that is responsible for the suppression of calcium-dependent inactivation (CDI). Thus, this channel exhibited CDI, compatible with a loss of function. In addition, the activation was shifted leftwards by -10 mV, indicating a gain of function. This complex phenotype could be rescued by coexpression of a C-terminal peptide comprised of 122 amino acids. Previous studies suggested that a shorter peptide should be sufficient to restore wild type properties. However, we did not observe any change in RX gating properties upon coexpression with this short eGFP-tagged peptide. We speculate that this may be due to steric hindrance of the big tag and further studies are necessary to resolve this issue.

The I745T (IT) mutation was found in a New Zealand family and causes a particularly severe form of CSNB2, as symptoms can also be found in heterozygous females and some hemizygous males show additional intellectual impairment. Functionally, the IT channels exhibited a dramatic leftward shift (-34 mV) in activation that results in a gain of function phenotype.

Taken together, these different mutations reflect the variety of $Ca_v1.4$ dysfunction phenotypes found in CSNB2 patients. As a consequence, these fundamental differences in the underlying functional defect have to be taken into account for future therapeutic approaches aiming to restore $Ca_v1.4$ wild type properties.

6.2. ZUSAMMENFASSUNG

Der L-Typ Kalziumkanal $Ca_v1.4$ wird beinahe ausschließlich in der Retina exprimiert, wo er Helligkeitsänderungen mit Glutamatfreisetzung koppelt. Um dieser Aufgabe gerecht zu werden, muss der Kanal lang anhaltenden Kalziumeinstrom vermitteln, was durch das Fehlen kalziumabhängiger Inaktivierung erreicht wird. Es sind verschiedene Mutationen in $Ca_v1.4$ bekannt, die eine kongenitale Form stationärer Nachtblindheit (CSNB2) verursachen. Es ist nicht bekannt, wie diese funktional sehr unterschiedlichen Mutationen die gleiche Krankheit hervorrufen können. In dieser Studie habe ich drei prototypische Mutationen untersucht, die in CSNB2 Patienten identifiziert wurden. Dazu habe ich diese Kanäle heterolog in tsA-201 Zellen exprimiert und ihre biophysikalischen Eigenschaften in elektrophysiologischen Experimenten ermittelt, um zu erforschen, wie diese Mutationen die Eigenschaften des Kanals verändern.

Die L216R (LR) Mutation, die im Spannungssensor des Kanals lokalisiert ist, verursachte einen „loss-of-function“ Phänotyp, da kein Kalziumeinstrom durch den Kanal detektiert werden konnte. Dies kann einerseits durch eine reduzierte Anzahl von Kanälen an der Zellmembran, andererseits durch nicht funktionale Kanäle erklärt werden. Wir konnten in einigen Zellen „gating current“ detektieren, was darauf hindeutet, dass Kanäle auf der Zelloberfläche vorhanden sind. Zusätzlich fanden wir eine Tendenz zu einem schnelleren Abbau von LR Kanälen. Zusammenfassend wird dieser Phänotyp wahrscheinlich durch funktionelle Entkopplung des Spannungssensors vom Öffnen der Pore verursacht, was zu einem Funktionsverlust von $Ca_v1.4$ führt.

Die R1827X (RX) Mutation führt dazu, dass die C-terminale Domäne fehlt, welche kalziumabhängige Inaktivierung in $Ca_v1.4$ unterdrückt. Daher zeigte dieser Kanal kalziumabhängige Inaktivierung, was einem „loss-of-function“ Phänotyp entspricht. Zusätzlich war die Aktivierung um -10mV nach links verschoben, was wiederum einem „gain-of-function“ Phänotyp gleichkommt. Wurde ein 122 Aminosäuren langes C-terminales Peptid koexprimiert, konnten die biophysikalischen Eigenschaften des Wildtyp-Kanals wiederhergestellt werden. Frühere Studien haben darauf hingedeutet, dass ein kürzeres Peptid ausreichen sollte, um diesen „rescue“ zu erreichen. Allerdings wurden die Eigenschaften des RX Kanals durch Koexpression dieses kürzeren eGFP-getaggten Peptids nicht verändert. Dies ist möglicherweise darauf zurückzuführe, dass dieser große eGFP-Tag die korrekte Interaktion des Peptides mit dem Kanal verhindert und weitere Untersuchungen sind vonnöten, um diese Frage zu beantworten.

Die I745T (IT) Mutation wurde in einer neuseeländischen Familie identifiziert und verursacht eine besonders schwere Form von CSNB2. In dieser Familie zeigen auch heterozygote Frauen Symptome und einige hemizygote Männer leiden zusätzlich unter kognitiven Beeinträchtigungen. Was die Funktion des IT Kanals betrifft, so zeigte sich ein dramatischer Linksshift (-34mV) der spannungsabhängigen Aktivierung, was in einem „gain-of-function“ Phäntyp resultiert.

Zusammenfassend lässt sich sagen, dass diese drei Mutationen die große Vielfalt an Phänotypen, die durch Mutationen in $Ca_v1.4$ entstehen und zu CSNB2 führen, repräsentieren. Folglich sind die zugrundeliegenden funktionalen Defekte höchst unterschiedlich und diese Unterschiede müssen für

zukünftige therapeutische Ansätze, die die Eigenschaften des Wildtyp-Kanals wieder herstellen sollen, berücksichtigt werden.

6.3. CURRICULUM VITAE

BIRGIT PÖHN

EDUCATION

Oct 2011 – 2014	University of Vienna, Faculty of Life Sciences, **Master of Science** in Molecular Biology with main focus on Neuroscience
Oct 2008 – Sep 2011	University of Veterinary Medicine Vienna, **Bachelor of Science** in Biomedicine and Biotechnology
Sep 2000 – June 2008	Bundesgymnasium und Bundesrealgymnasium Gmünd

PROFESSIONAL EXPERIENCE

Feb 2013 – 2014	**Master Thesis:** Medical University Vienna, Center for Physiology and Pharmacology, Department of Neurophysiology and Neuropharmacology
Supervisor:	Univ. Prof. Mag. Dr. Alexandra Koschak
Title of thesis:	Different phenotypes of $Ca_v1.4$ loss-of-function mutations
Oct 2011 – Feb 2013	University of Veterinary Medicine Vienna, Institute of Medical Biochemistry, **laboratory technician** (part-time employment)
Supervisor:	Dipl.-Biol. Dr. rer. nat. Rudolf Moldzio
March – July 2011	**Bachelor Thesis**: University of Veterinary Medicine Vienna, Institute of Medical Biochemistry
Supervisor:	Dipl.-Biol. Dr. rer. nat. Rudolf Moldzio
Title of thesis:	Cannabinoids as neuroprotective agents in cellular rotenone-models of Parkinson's disease

POSTERS

International Congress on Natural Products Research (ICNPR) 2012, New York City.

Pöhn B, Krewenka C, Kranner B, Duvigneau JC, Rausch WD, Moldzio R.

Phytocannabinoids tetrahydrocannabinol and cannabidiol act against rotenone induced damages in murine cell cultures. Planta Med (78), 1110

5. ÖGMBT Jahrestagung 2013, Innsbruck.

Burtscher V, **Pöhn B**, Schicker KW, Korkmaz S, Singh A, Janecke A, Blatsios G, Koschak A.

Different loss-of-function phenotypes in $Ca_v1.4$ L-type calcium channel mutants from CSNB2 patients.

PUBLICATIONS

Burtscher V, Schicker KW, Novikova E, **Pöhn B**, Stockner T, Kugler C, Singh A, Zeitz C, Lancelot ME, Audo I, Leroy BP, Freissmuth M, Herzig S, Matthes J, Koschak A (2014)

Spectrum of $Ca_v1.4$ dysfunction in congenital stationary night blindness type 2.

BBA - Biomembranes, **1838**, 2053–2065